SIAM J. APPL. MATH.
Vol. 78, No. 2, pp. 1174–1205
© 2018 Society for Industrial and Applied Mathematics

Downloaded 04/19/18 to 129.67.185.193. Redistribution subject to SIAM license or copyright; see http://www.siam.org/journals/ojsa.php

ASYMPTOTIC ANALYSIS OF A SILICON FURNACE MODEL*

BENJAMIN M. SLOMAN†, COLIN P. PLEASE†, AND ROBERT A. VAN GORDER†

Abstract. Silicon is produced from quartz rock in electrode-heated furnaces by using carbon as a reduction agent. We perform an asymptotic analysis of a heat and mass transfer model of an experimental pilot furnace in order to determine the dominant chemical and thermal behavior of the system. First, by prescribing a steady-state temperature profile in the furnace we explore the leading order reactions in different spatial regions, as well as early time behavior. We are able to obtain asymptotic solutions which compare well with numerical simulations. Utilizing the dominant balances found when the temperature is prescribed, we next reduce the full model to two coupled partial differential equations for the time-variable temperature profile within the furnace and the concentration of solid quartz. These equations account for diffusion, an endothermic reaction, and the external heating input to the system. A moving boundary is found and the behavior on either side of this boundary explored in the asymptotic limit of small diffusion. We note how the simplifications derived may be useful for future models and industrial furnace operation and comment on insights from the model about furnace crust formation.

Key words. heat and mass transfer, silicon furnace, endothermic reaction, asymptotic analysis, multiple scales, moving boundary problems

AMS subject classifications. 80A20, 92E20, 80M35, 35R37

DOI. 10.1137/17M1122335

1. Introduction.

Silicon is an important material, being used in crystal form for semiconductors in solar panels and computers, as polysilicon in such things as paint and textiles, and as part of metallic alloys [17]. It is produced from the raw material quartz (SiO_2), using carbon as a reduction agent, in large furnaces which are heated by electrodes [2, 11, 17, 21]. In the furnaces numerous chemical reactions occur, as well as different types of interactions between solid, liquid, and gaseous phases. The high temperatures found (around 2000 K) are influenced by the chemical reactions and the electrical heating. Mathematical modeling is crucial to understand the interdependence between the physical and chemical effects taking place. In furnace operation a crust emerges, comprising solid and viscous liquid substances, preventing raw material from reaching the hotter, lower part of the furnace and hence inhibiting the necessary reactions from taking place. To counter this the furnace is "stoked" on an hourly basis, whereby the crust is manually broken up. This is a tedious operation, and thus it is of particular interest to see if this crust formation can be understood better. In [20] we produced a continuum model of a silicon furnace, simplifying the geometry to replicate a pilot furnace experiment. Here we build on this work by examining asymptotic limits of this model, in order to capture and better understand the underlying behavior.

There is a wealth of mathematical literature on problems of coupled chemical and thermal effects. In [4, 13, 15] the authors consider catalytic converters and combustion. Here an exothermic reaction heats the system, causing an initial light-off behavior [15]

*Received by the editors March 23, 2017; accepted for publication (in revised form) February 13, 2018; published electronically April 17, 2018.
http://www.siam.org/journals/siap/78-2/M112233.html
Funding: This work was supported by the EPSRC Center for Doctoral Training in Industrially Focused Mathematical Modelling (EP/L015803/1). The first author received financial support from Elkem.

†Mathematical Institute, University of Oxford, Andrew Wiles Building, Radcliffe Observatory Quarter, Woodstock Road, Oxford, OX2 6GG, United Kingdom (Ben.Sloman@maths.ox.ac.uk, Colin.Please@maths.ox.ac.wk, Robert.VanGorder@maths.ox.ac.uk).

Copyright © by SIAM. Unauthorized reproduction of this article is prohibited.

Downloaded 04/19/18 to 129.67.185.193. Redistribution subject to SIAM license or copyright; see http://www.siam.org/journals/ojsa.php

and the mechanisms by which the reaction switches off [4] are studied by asymptotic means. A separate, but linked, body of work examines competing exothermic and endothermic reactions [7, 16, 19, 23]. If there is just a single exothermic reaction, or two exothermic reactions, traveling wave solutions exist. However, the presence of the endothermic reaction, removing heat from the system, means these traveling waves can exist only for certain regions of the parameter space. In [3] premixed flames are considered and in [1] a model of coupled heat transfer and an endothermic reaction is analyzed. Useful analogues of the behavior in the model of Sloman et al. [20] can be found in work set in different physical contexts. In [5] the authors find a moving drying front in the roasting of a coffee bean, which separates a dry region from a preheating region. The behavior of this narrow transition region is analyzed using asymptotic methods. The processing of glass in a furnace is considered in [6], where a melted upper region and an unmelted lower batch region are separated by a downward moving traveling front. In the context of tumor cells the authors of [12] find new discontinuous traveling waves for different hyperbolic PDE models. Although many chemical processes contain numerous reactions, it is possible to reduce the number of equations in mathematical models describing these processes by making certain simplifications. One of these is the quasi-steady-state assumption [18] or pseudo-steady-state hypothesis. There is a separation of timescales, so that after the initial fast timescale some of the variables can be assumed to be in steady state, reducing the number of equations to be solved to find the other variables, which vary over a longer timescale.

In section 2 we present a summary of the model for a silicon furnace developed in [20], listing equations in dimensional variables and giving brief descriptions of what these represent physically. We nondimensionalize this model in such a way as to ensure all dimensionless variables are order one in size, while parameters are also order one, except for two which are small. In section 3 we examine this model with the simplification of a prescribed steady-state temperature profile in the limit of these small parameters going to zero. This corresponds physically to the reaction between liquid quartz and carbon being instantaneous when compared to the melting of solid quartz and gas advection being instantaneous when compared to both these effects. Using a prescribed temperature profile makes the leading order system of equations easier to solve and allows us to capture the behavior of the dominant chemical effects. We find that two spatial regions emerge: a lower, hot region where gas is produced from the solid carbon and quartz, and a cold, upper region where SiO gas reacts with carbon particles and also condenses. We also find two timescales, with an initial fast transience followed by a slower outer timescale. In section 4 we consider asymptotics of the full problem, where the varying temperature is coupled with chemistry and gas transport. We find that the leading order problem comprises an endothermic chemical reaction acting as a sink in the heat equation, which has an external source. This differs from much of the literature discussed, which largely deals with exothermic reactions (e.g., [4, 13, 15]). We find spatial regions similar to those which arise in section 3 with a prescribed temperature profile, with the difference that the spatial interface rises in the furnace with a traveling wave type behavior. We are particularly interested in both crust formation and the interface between the charge and the gas cavity, given in this model by the isotherm where quartz begins to melt. There is discussion of the melting isotherm throughout sections 3 and 4, and in section 5 we give insights into crust formation. Concluding remarks are given in section 6.

2. The model. We take the model for a silicon furnace from [20]. This is a continuum model for the dynamics of chemical concentrations, gas partial pressures,

Copyright © by SIAM. Unauthorized reproduction of this article is prohibited.

material transport, and temperature within a vertical section of a furnace. The model is applied to pilot furnace experiments, discussed in [20], and so electrical effects are not considered. Heat transfers due to gas advection, conduction, radiation, exothermic and endothermic reaction heat release or absorption, and an external energy source. Diffusion of gases is neglected due to the high Péclet number (around 10^3), and for simplicity solids and liquids move in a constant bulk flow. We give a summary of the model here, but further details are found in [20].

The model assumes that at any point in the furnace there is a mixture of one of seven chemical species. These are three solid species: carbon (C), silicon carbide (SiC), and quartz (SiO_2(s)); two liquid species: "sticky" quartz (SiO_2(l)) and silicon (Si); and two gaseous species: carbon monoxide (CO) and silicon monoxide (SiO). The model considers the effective concentration of these chemicals, denoted C_X [mol/m^3] for each species X. This gives the number of moles of X per unit volume of the mixture of all species in the furnace. All the solids, liquids, and gases are considered to be locally at the same varying temperature T [K], and there are assumed to be no voids in the furnace, so that any arbitrary volume is filled with a combination of the chemical species modeled. The total gas pressure P_{TOT} is assumed to be constant, at 1 bar, created by the partial pressure of silicon monoxide, denoted P, and carbon monoxide. Both gases are allowed to move at the same varying velocity $\mathbf{V}_g = U_g\mathbf{k}$. Advection of gases dominates over diffusion, so gas diffusion is not included in the model. The imposition of constant total pressure and a no-voids condition means that gas moves in order to equilibrate pressure. If gas is produced through reactions in one part of the furnace, then it will move away from that region to keep the total pressure steady. Thus the gas velocity is not explicitly stated but is determined implicitly as part of the model. The solids and liquids are assumed to move at a constant velocity $\mathbf{V}_s = -U_s\mathbf{k}$. We apply our model to the pilot furnace experiments, described in [20], and so take U_s to be zero since material is not fed in to the furnace top during the experiments. As can be seen in Figure 1, the prevailing structure in the pilot furnace is unidimensional. We are interested in the location of crust formation, and this can be captured using a single spatial coordinate z, representing height in the furnace. Although the gas cavity and the crater are distinct regions in experimental and industrial furnaces, since we have a mixture of solids, liquids, and gases at all heights these regions are combined in our model, with the joint region referred to as the base of the furnace.

The following chemical reactions are considered to take place in the furnace, with bracketed notation (s) denoting a solid, (l) a liquid, and (g) a gas:

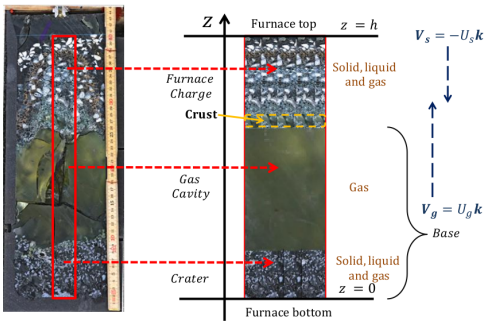

FIG. 1. *The red box in the left-hand image shows a typical vertical section in the pilot furnace. The horizontal variations are smoothed out in the right-hand image to illustrate the approximation of the furnace geometry with a one-dimensional model. Reproduced from* [20].

Downloaded 04/19/18 to 129.67.185.193. Redistribution subject to SIAM license or copyright; see http://www.siam.org/journals/ojsa.php

Copyright © by SIAM. Unauthorized reproduction of this article is prohibited.

Downloaded 04/19/18 to 129.67.185.193. Redistribution subject to SIAM license or copyright; see http://www.siam.org/journals/ojsa.php

$$\mathrm{SiO(g)} + 2\mathrm{C(s)} \xrightarrow{R_1} \mathrm{SiC(s)} + \mathrm{CO(g)}, \tag{1}$$

$$2\mathrm{SiO(g)} \underset{R_{-2}}{\overset{R_2}{\rightleftharpoons}} \mathrm{SiO_2(l)} + \mathrm{Si(l)}, \tag{2}$$

$$\mathrm{SiO_2(s)} \xrightarrow{R_3} \mathrm{SiO_2(l)}, \tag{3}$$

$$\mathrm{SiO(g)} + \mathrm{SiC(s)} \xrightarrow{R_4} 2\mathrm{Si(l)} + \mathrm{CO(g)}, \tag{4}$$

$$\mathrm{SiO_2(l)} + \mathrm{C(s)} \xrightarrow{R_5} \mathrm{SiO(g)} + \mathrm{CO(g)}. \tag{5}$$

Using the relations $\mathrm{C_{CO}} + \mathrm{C_{SiO}} = \mathrm{C}_g$, $\mathrm{C_{CO}} = \mathrm{C}_g(P_{\mathrm{TOT}} - P)$, and $\mathrm{C_{SiO}} = \mathrm{C}_g P$, the dimensional model equations are

$$\begin{aligned}
&\frac{\partial}{\partial t}\begin{pmatrix} \mathrm{C_C} \\ \mathrm{C_{SiC}} \\ \mathrm{C_{SiO_2(s)}} \\ \mathrm{C_{SiO_2(l)}} \\ \mathrm{C_{Si}} \\ \mathrm{C}_g(P_{\mathrm{TOT}} - P) \\ \mathrm{C}_g P \end{pmatrix} + \frac{\partial}{\partial z}\begin{pmatrix} -U_s\mathrm{C_C} \\ -U_s\mathrm{C_{SiC}} \\ -U_s\mathrm{C_{SiO_2(s)}} \\ -U_s\mathrm{C_{SiO_2(l)}} \\ -U_s\mathrm{C_{Si}} \\ U_g\mathrm{C}_g(P_{\mathrm{TOT}} - P) \\ U_g\mathrm{C}_g P \end{pmatrix} \\
&= \begin{pmatrix} -2 & 0 & 0 & 0 & 0 & -1 \\ 1 & 0 & 0 & 0 & -1 & 0 \\ 0 & 0 & 0 & -1 & 0 & 0 \\ 0 & 1 & -1 & 1 & 0 & -1 \\ 0 & 1 & -1 & 0 & 2 & 0 \\ 1 & 0 & 0 & 0 & 1 & 1 \\ -1 & -2 & 2 & 0 & -1 & 1 \end{pmatrix}\begin{pmatrix} R_1 \\ R_2 \\ R_{-2} \\ R_3 \\ R_4 \\ R_5 \end{pmatrix},
\end{aligned} \tag{6}$$

$$\frac{RT\mathrm{C}_g}{P_{\mathrm{TOT}}} + \sum_{\text{solids and liquids } i} \mathrm{C_i}\frac{M_{\mathrm{i}}}{\rho_{\mathrm{i}}} = 1, \tag{7}$$

$$\begin{aligned}
&\frac{\partial}{\partial t}\left(T\left(A_f(\sigma_s + \sigma_g) + A_{gr}\sigma_{gr}\right)\right) + \frac{\partial}{\partial z}\left(TA_f\left(-U_s\sigma_s + U_g\sigma_g\right)\right) \\
&= \frac{\partial}{\partial z}\left(\left(A_f k_f + A_{gr}k_{gr}\right)\frac{\partial T}{\partial z} + A_f\beta T^3\frac{\partial T}{\partial z}\right) + A_f\sum_j dH_j R_j + \left(A_f + A_{gr}\right)F,
\end{aligned} \tag{8}$$

where

$$\begin{pmatrix} R_1 \\ R_2 \\ R_{-2} \\ R_3 \\ R_4 \\ R_5 \end{pmatrix} = \begin{pmatrix} k_1\mathrm{r_C}\mathrm{C_C}(P - P_1(T))^+ \\ k_2(P - P_2(T))^+ \\ k_{-2}\mathrm{C_{SiO_2(l)}}\mathrm{C_{Si}} \\ k_3\mathrm{C_{SiO_2(s)}}(T - T_M)^+ \\ k_4\mathrm{C_{SiC}}(P - P_4(T))^+ \\ k_5\mathrm{C_{SiO_2(l)}}\mathrm{C_C} \end{pmatrix}. \tag{9}$$

Here we have denoted $R = 8.314$ J/molK as the gas constant, M_i the molar mass of each species, and ρ_i the corresponding species density, assumed to be constant for solids and liquids. A_f and A_{gr} are the cross-sectional surface areas of the pilot furnace and graphite crucible, respectively, σ_s, σ_g, and σ_{gr} are the heat capacities in the solid and liquid material, the gas, and the graphite crucible, k_f and k_{gr} are the effective

Copyright © by SIAM. Unauthorized reproduction of this article is prohibited.

Downloaded 04/19/18 to 129.67.185.193. Redistribution subject to SIAM license or copyright; see http://www.siam.org/journals/ojsa.php

thermal conductivity of material inside the pilot furnace and the graphite crucible, with β a radiative constant associated with radiation between furnace particles, estimated assuming black body radiation and a typical distance between solid particles of 1 mm. dH_j is the rate of heat release for reaction j (and is negative for endothermic reactions). $F(z)$ is a function representing external heating into the graphite crucible from the induction heater. For simplicity, in the model analysis in [20] this function was taken to be $F(z) = Q\mathcal{H}(h_T - z)$, where Q is a scalar representing the heating strength per unit volume, $\mathcal{H}$ is the Heaviside function, and the pilot furnace is being heated up to some fixed height h_T. In section 4.1 we will use this function to ease the analysis of the resulting series solution. However, a different functional form of $F(z)$ could readily be used, and in particular in sections 4.2 and 4.3 our asymptotic solutions require an invertible $F(z)$. When a specific heating profile is needed in these sections we will use the smooth function $F(z) = \frac{Q}{2}\left(1 + \tanh(\mu(h_T - z))\right)$, which tends to a multiple of the Heaviside function as $\mu \to \infty$. The k_j in (9) are reaction constants, and the $P_j(T)$ are partial pressure functions of temperature, which limit the appropriate reactions. Note that $\mathrm{r_C}$ represents the reactivity of carbon, which could vary with different raw materials used and also during furnace operation. For simplicity, in this model $\mathrm{r_C}$ is taken to be a constant between zero and one. Similarly, for simplicity, the contact surface is not considered in reactions R_{-2}, R_4, or R_5, which are between two liquids, a gas and a solid, and a liquid and a solid, respectively. Finally, $T_M = 1996$ K is the dimensional melting temperature of quartz [2]. Several of the reaction rates in (9) are not smooth. As can be seen in Figure 7 of paper [20], for such reactions the spatial domain is divided into regions where the reaction occurs and where it does not occur. This is exploited in section 3 of this paper.

From now on we take $U_s = 0$, since we consider behavior within the pilot furnace experiment where material is not fed in to the top of the furnace. Our model has the initial conditions

$$\mathrm{C_C} = c_0, \quad \mathrm{C_{SiC}} = 0, \quad \mathrm{C_{SiO_{2(s)}}} = c_0\alpha, \ \mathrm{C_{SiO_{2(l)}}} = 0, \ \mathrm{C_{Si}} = 0, \ P = \frac{P_{\mathrm{TOT}}}{2},$$

$$U_g = 0, \ T = 300, \ \mathrm{C}_g = \frac{P_{\mathrm{TOT}}}{300R}\left(1 - c_0\left(\frac{M_{\mathrm{C}}}{\rho_{\mathrm{C}}} + \frac{M_{\mathrm{SiO_2}(s)}}{\rho_{\mathrm{SiO_2}(s)}}\alpha\right)\right), \tag{10}$$

at $t = 0$, where $c_0 = 38000$ mol/m^3 and $\alpha = 0.454$ are measured from the experiment. We also have the boundary conditions

$$U_g(0,t) = 0, \quad \frac{\partial T(0,t)}{\partial z} = 0, \quad \frac{\partial T(1,t)}{\partial z} = 0. \tag{11}$$

Note there is no boundary condition for $U_g(1,t)$ because gas is free to leave the top of the furnace.

In [20] we performed numerical simulations of this model to replicate behavior in the pilot furnace and conducted parameter sweeps to see the influence of various input parameters on output metrics of the silicon yield, the SiO losses, and solid buildup. As in [20], all numerical simulations in this paper are found using first order finite difference schemes, with upwinding for convective fluxes and the timestep chosen to obey the Courant–Friedrichs–Lewy condition. There is, however, much to be learned by exploiting the relative sizes of the various parameters that are found in the model to determine the asymptotic behavior. Many of the parameters in the model are not known accurately but have been calibrated with industrial furnaces to give sensible results from previous models (see the dynamic model [8] and SiMod [22]). Thus

Copyright © by SIAM. Unauthorized reproduction of this article is prohibited.

finding the general qualitative behavior when certain parameters are small or large helps to understand the interplay of the chemical, thermal, and transport effects.

We choose to write the dimensionless model in terms of the timescale of the melting reaction R_3, $\tau = (k_3 T_0)^{-1}$, where $T_0 = 1000$ K is the typical temperature difference between the top and bottom of the furnace. In the numerical simulations shown in [20] we find that the concentrations of SiC, SiO_2(l), and Si remain around 30 times smaller than the concentrations of C and SiO_2(s). Also, the concentration of gas is around 10^4 times smaller than the concentrations of C and SiO_2(s). We thus seek parameters ϵ and δ such that the concentrations of SiC, SiO_2(l), and Si are $\mathcal{O}(\epsilon)$, and the concentration of gas is $\mathcal{O}(\delta)$. A scale for ϵ emerges by considering a balance between reactions R_3 and R_5. Liquid quartz is formed through R_3 and then reacts with C through R_5 to form CO and SiO. We let ϵ be the ratio of the rate of R_3 to R_5 or ratio of the timescale of R_5 to R_3. We let δ be the ratio of time taken for the gas to convect the height of the furnace to the timescale for R_3. We thus have

$$\epsilon = \frac{k_3 T_0}{k_5 c_0} = \frac{1/k_5 c_0}{1/k_3 T_0}, \quad \delta = \frac{h/V}{1/k_3 T_0}, \tag{12}$$

where h is the height of the furnace and V is a typical value of the magnitude of the gas velocity. We have $0 < \delta \ll \epsilon \ll 1$ and will consider the joint limits $\epsilon \to 0$ and $\delta \to 0$, with $\delta/\epsilon \to 0$. The limit $\epsilon \to 0$ corresponds to the reaction between carbon and SiO_2(l) being instantaneous when compared to the melting of SiO_2(l), so that as soon as quartz melts to liquid quartz it reacts with any available carbon. The limit $\delta \to 0$ corresponds to instantaneous gas flow when compared with the melting of quartz, but as $\delta/\epsilon \to 0$, this gas flow is also faster than the chemical timescale for R_5.

We thus utilize the dimensionless scalings

$$\begin{aligned}
&\mathrm{C_C} = c_0 \bar{\mathrm{C}}_\mathrm{C}, \quad \mathrm{C}_{\mathrm{SiO_2(s)}} = c_0 \bar{\mathrm{C}}_{\mathrm{SiO_2(s)}}, \quad \mathrm{C_{SiC}} = \epsilon c_0 \bar{\mathrm{C}}_{\mathrm{SiC}}, \quad \mathrm{C}_{\mathrm{SiO_2(l)}} = \epsilon c_0 \bar{\mathrm{C}}_{\mathrm{SiO_2(l)}},\\
&\mathrm{C_{Si}} = \epsilon c_0 \bar{\mathrm{C}}_{\mathrm{Si}}, \quad \mathrm{C_g} = \delta c_0 \bar{\mathrm{C}}_\mathrm{g}, \ T = (T_{\mathrm{bottom}} - T_{\mathrm{top}})\bar{T} + T_{\mathrm{top}}, \ t = \tau \bar{t}, \ z = h\bar{z},\\
&U_g = V \bar{U}_g, \quad P = P_{\mathrm{TOT}} \bar{P}, \quad P_j = P_{\mathrm{TOT}} \bar{P}_j, \quad \sigma_s = c_0 C_{p,C} \bar{\sigma}_s,\\
&\sigma_g = \delta c_0 C_{p,C} \bar{\sigma}_g, \quad F(z) = Q \bar{F}(\bar{z}),
\end{aligned} \tag{13}$$

where $T_{\mathrm{bottom}} = 2400$ K and $T_{\mathrm{top}} = 1400$ K are typical temperatures found at the bottom and the top of the furnace, and $C_{p,C}$ is the specific heat of carbon. Dropping the overbar notation we have the dimensionless equations

$$\begin{aligned}
&\frac{\partial}{\partial t}\begin{pmatrix} \mathrm{C_C} \\ \epsilon \mathrm{C_{SiC}} \\ \mathrm{C}_{\mathrm{SiO_2(s)}} \\ \epsilon \mathrm{C}_{\mathrm{SiO_2(l)}} \\ \epsilon \mathrm{C_{Si}} \\ \delta \mathrm{C}_g(1-P) \\ \delta \mathrm{C}_g P \end{pmatrix} + \frac{\partial}{\partial z}\begin{pmatrix} 0 \\ 0 \\ 0 \\ 0 \\ 0 \\ U_g \mathrm{C}_g(1-P) \\ U_g \mathrm{C}_g P \end{pmatrix}\\
&= \begin{pmatrix} -2 & 0 & 0 & 0 & 0 & -1 \\ 1 & 0 & 0 & 0 & -1 & 0 \\ 0 & 0 & 0 & -1 & 0 & 0 \\ 0 & 1 & -1 & 1 & 0 & -1 \\ 0 & 1 & -1 & 0 & 2 & 0 \\ 1 & 0 & 0 & 0 & 1 & 1 \\ -1 & -2 & 2 & 0 & -1 & 1 \end{pmatrix} \begin{pmatrix} \epsilon r_1 \\ \epsilon r_2 \\ \epsilon r_{-2} \\ r_3 \\ \epsilon r_4 \\ r_5 \end{pmatrix},
\end{aligned} \tag{14}$$

Copyright © by SIAM. Unauthorized reproduction of this article is prohibited.

Downloaded 04/19/18 to 129.67.185.193. Redistribution subject to SIAM license or copyright; see http://www.siam.org/journals/ojsa.php

Downloaded 04/19/18 to 129.67.185.193. Redistribution subject to SIAM license or copyright; see http://www.siam.org/journals/ojsa.php

$$g_0\left(T+\frac{T_{\rm top}}{T_0}\right)\mathrm{C}_g+m_{\rm C}\mathrm{C}_{\rm C}+\epsilon m_{\rm SiC}\mathrm{C}_{\rm SiC}+m_{\mathrm{SiO_2(s)}}\mathrm{C}_{\mathrm{SiO_2(s)}}+\epsilon m_{\mathrm{SiO_2(l)}}$$

$$+\mathrm{C}_{\mathrm{SiO_2(l)}}+\epsilon m_{\rm Si}\mathrm{C}_{\rm Si}=1, \tag{15}$$

$$\frac{\partial}{\partial t}\left(\left(T+\frac{T_{top}}{T_0}\right)\left(\sigma_s+\delta\sigma_g+\sigma_{gr}^*\right)\right)+\frac{\partial}{\partial z}\left(\left(T+\frac{T_{top}}{T_0}\right)U_g\sigma_g\right)$$
$$=a\frac{\partial^2 T}{\partial z}+\beta^*\frac{\partial}{\partial z}\left(\left(\frac{T_{top}}{T_0}+T\right)^3\frac{\partial T}{\partial z}\right)+\epsilon\left(\gamma_1 r_1+\gamma_2 r_2+\gamma_{-2}r_{-2}+\gamma_4 r_4\right)+\gamma_5 r_5+qF, \tag{16}$$

where

$$\begin{pmatrix} r_1\\ r_2\\ r_{-2}\\ r_3\\ r_4\\ r_5\end{pmatrix}=\begin{pmatrix}\chi_1\mathrm{C}_{\rm C}(P-P_1(T))^+\\ \chi_2(P-P_2(T))^+\\ \chi_{-2}\mathrm{C}_{\mathrm{SiO_2(l)}}\mathrm{C}_{\rm Si}\\ \mathrm{C}_{\mathrm{SiO_2(s)}}(T-T_m)^+\\ \chi_4\mathrm{C}_{\rm SiC}(P-P_4(T))^+\\ \mathrm{C}_{\mathrm{SiO_2(l)}}\mathrm{C}_{\rm C}\end{pmatrix}, \tag{17}$$

$$\sigma_s=\mathrm{C}_{\rm C}+\epsilon\mathrm{C}_{\rm SiC}C_{P,\mathrm{SiC/C}}+\mathrm{C}_{\mathrm{SiO_2(s)}}C_{P,\mathrm{SiO_2(s)/C}}+\epsilon\mathrm{C}_{\mathrm{SiO_2(l)}}C_{P,\mathrm{SiO_2(l)/C}}+\epsilon\mathrm{C}_{\rm Si}C_{P,\mathrm{Si/C}}, \tag{18}$$

$$\sigma_g=\mathrm{C}_g\left((1-P)C_{P,\mathrm{CO/C}}+PC_{P,\mathrm{SiO/C}}\right),\quad g_0=\delta\frac{RT_0c_0}{P_{\rm TOT}},\quad m_{\rm X}=c_0\frac{M_{\rm X}}{\rho_{\rm X}}. \tag{19}$$

We have scaled the kinetic rates χ_j such that each is an order one constant, taking a typical value $\mathrm{r_C}=0.2$ [20] when choosing the appropriate scale for r_1. Each variable and parameter listed in the equations above is order one. g_0 is an order one constant, since $RT_0c_0/P_{\rm TOT}$ is $\mathcal{O}(\delta^{-1})$ with $T_0:=T_{\rm bottom}-T_{\rm top}$, as are the $m_{\rm X}$. We have used the shorthand notation $C_{P,\mathrm{X/C}}:=C_{P,\mathrm{X}}/C_{P,\mathrm{C}}$ in the heat capacities σ_s and σ_g. T_m is the dimensionless melting temperature of quartz. There is no heat release associated with r_3 in the model, so there is no γ_3.

We have the dimensionless initial conditions (for $0\le z\le 1$)

$$\mathrm{C}_{\rm C}=1,\quad \mathrm{C}_{\rm SiC}=0,\quad \mathrm{C}_{\mathrm{SiO_2(s)}}=\alpha,\quad \mathrm{C}_{\mathrm{SiO_2(l)}}=0,\quad \mathrm{C}_{\rm Si}=0,\quad P=\frac{1}{2},$$
$$U_g=0,\quad T=-1.1,\quad \mathrm{C}_g=\frac{P_{\rm TOT}}{300R}\left(\frac{1}{c_0}-\left(\frac{M_{\rm C}}{\rho_{\rm C}}+\frac{M_{\mathrm{SiO_2(s)}}}{\rho_{\mathrm{SiO_2(s)}}}\alpha\right)\right), \tag{20}$$

at $t=0$, with the dimensionless boundary conditions remaining the same as the dimensional boundary conditions given in (11).

To understand the behavior of solutions to our model (14)–(20) we begin by constraining the temperature to be fixed, with a prescribed steady-state temperature $T(z)$ considered in section 3, and we neglect the energy equation (16). Although neither pilot or industrial furnaces operate with a steady-state temperature, this allows us to focus on the chemical and gas transport dynamics and makes the analysis more tractable. In section 4 we will return to the problem with time-variable temperature. Although less analytical progress can then be made, the simplifications developed allow for a reduced model to be identified.

3. Prescribed temperature asymptotics. We analyze the dimensionless equations (14)–(15), but with a prescribed temperature profile $T(z)$ instead of the energy equation (16). Initial conditions (20) and boundary conditions (11) are used

Copyright © by SIAM. Unauthorized reproduction of this article is prohibited.

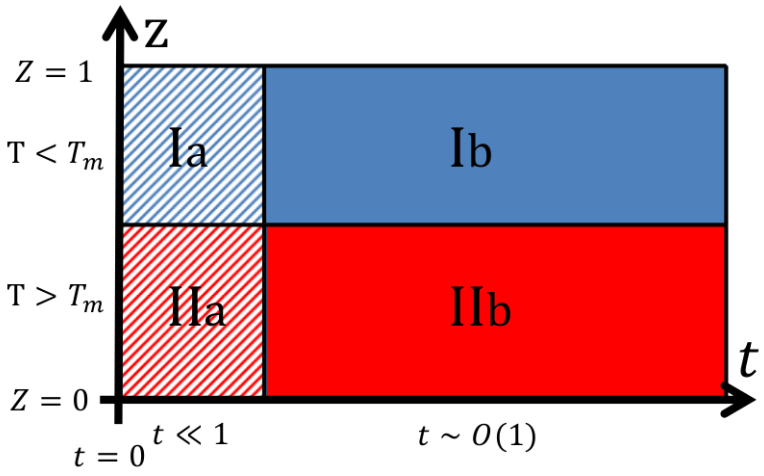

FIG. 2. *Schematic of asymptotic regimes. Hashed regions correspond to early time and solid regions to larger time. The blue region, where the temperature is below the melting point of quartz, corresponds to the furnace charge. The red region, where melting of quartz occurs, corresponds to the mixed cavity and crater region in the model.*

for concentrations, partial pressure, and gas velocity. Where possible we will work in terms of a general $T(z)$, but any time a specific profile is used we will utilize the piecewise linear profile $T(z) = \min(1, \frac{1-z}{1-h_T^*})$. With this function the furnace is at constant unitary temperature up to a dimensionless height $h_T^* = 0.544$ and above this height linearly decays to zero at the top of the furnace. This is to replicate the experimental behavior, where the induction furnace creates a temperature gradient by inputting more heat into the bottom of the furnace (see [20]).

There are different spatial regions in the problem, due to the behavior of the melting reaction $r_3 = \mathrm{C}_{\mathrm{SiO_2(s)}}(T - T_m)^+$. In the lower, hotter part of the furnace $T > T_m$ and hence $r_3 = \mathcal{O}(1)$. In the upper, colder region of the furnace $T < T_m$ and hence $r_3 = 0$. These regions are separated by the interface given by the isotherm $T = T_m$. With a prescribed temperature profile we do not consider any temperature transient as it heats from cold, but start the process from the prescribed hot profile. Hence the chemistry has a rapid transient period before getting near typical operating conditions. There are thus four main regimes of behavior of the chemistry in height-time space, which are shown in Figure 2.

There is a separation between the blue region, where the temperature is too cold for solid quartz to melt, and the red region, where quartz melts. There is also a separation between the early time regions (shown as hashed), where the pilot furnace moves away from the initial conditions to dynamics more likely to be seen in the industrial furnace, and the $\mathcal{O}(1)$ time regions (shown as solid). Since in all practical situations $U_g \geq 0$, and we have assumed no solid or liquid motion, we have that information propagates upward in Figure 2 (so from Region II to Region I) as well as rightward (from Region a to Region b). We now give details of the behavior in each region found through expanding each variable in terms of the small parameter ϵ. That is, for a variable Y we have $Y = Y^0 + \epsilon Y^1 + \mathcal{O}(\epsilon^2)$. We begin by considering Region II, since the gas produced in this region influences the dynamics in Region I. We find analytic solutions in Regions IIa and IIb and, where appropriate, give composite solutions that replicate both the inner and outer time behavior. We then

Copyright © by SIAM. Unauthorized reproduction of this article is prohibited.

Downloaded 04/19/18 to 129.67.185.193. Redistribution subject to SIAM license or copyright; see http://www.siam.org/journals/ojsa.php

Downloaded 04/19/18 to 129.67.185.193. Redistribution subject to SIAM license or copyright; see http://www.siam.org/journals/ojsa.php

examine the upper part of the furnace, which is Region I. In Region Ia we list the leading order equations but find that the solid and liquid concentrations are solved by the initial conditions. Hence the corresponding leading order equations arising in Region Ib can be solved with these initial conditions, and analytic solutions are found for all of Region I. Matching occurs between Regions I and II in terms of continuity of the gas flux across the interface $T = T_m$. We give a summary of the main asymptotic behavior in each region but do not include all the details. A summary of leading and first order solutions is given in the appendix.

3.1. Region IIa—early time cavity and crater. We find that the appropriate timescale is $t = \epsilon\hat{t}$, where $\hat{t}$ is an order one variable. With this rescaling we find that the leading order equations from the matrix system (14) are at $\mathcal{O}(\epsilon^{-1})$ and are given by

$$\frac{1}{\epsilon}\frac{\partial \mathrm{C}_{\mathrm{C}}^0}{\partial \hat{t}} = \mathcal{O}(1), \quad \frac{1}{\epsilon}\frac{\partial \mathrm{C}_{\mathrm{SiO_2(s)}}^0}{\partial \hat{t}} = \mathcal{O}(1), \tag{21}$$

which have solutions $\mathrm{C}_{\mathrm{C}}^0 = 1$ and $\mathrm{C}_{\mathrm{SiO_2(s)}}^0 = \alpha$. We use these when finding the leading order terms for the other variables. For the concentrations of SiC, SiO_2(l), and Si we have

$$\frac{\partial \mathrm{C}_{\mathrm{SiC}}^0}{\partial \hat{t}} = \mathcal{O}(\epsilon), \quad \frac{\partial \mathrm{C}_{\mathrm{SiO_2(l)}}^0}{\partial \hat{t}} = \alpha(T - T_m) - \mathrm{C}_{\mathrm{SiO_2(l)}}^0 + \mathcal{O}(\epsilon), \quad \frac{\partial \mathrm{C}_{\mathrm{SiC}}^0}{\partial \hat{t}} = \mathcal{O}(\epsilon). \tag{22}$$

With the zero initial conditions we have $\mathrm{C}_{\mathrm{SiC}}^0 = 0$, $\mathrm{C}_{\mathrm{Si}}^0 = 0$, and

$$\mathrm{C}_{\mathrm{SiO_2(l)}}^0 = \alpha\left(T(z) - T_m\right)\left(1 - e^{-\hat{t}}\right) = \alpha\left(T(z) - T_m\right)\left(1 - e^{-t/\epsilon}\right). \tag{23}$$

We can find the leading order gas flux $U_g^0\mathrm{C}_g^0$ and pressure P^0 from the equations

$$\frac{\partial}{\partial z}\left(U_g^0\mathrm{C}_g^0(1 - P^0)\right) = \mathrm{C}_{\mathrm{SiO_2(l)}}^0 + \mathcal{O}(\epsilon), \quad \frac{\partial}{\partial z}\left(U_g^0\mathrm{C}_g^0 P^0\right) = \mathrm{C}_{\mathrm{SiO_2(l)}}^0 + \mathcal{O}(\epsilon). \tag{24}$$

Utilising the no-flux boundary condition $U_g(0, \hat{t}) = 0$, we can add the above equations and integrate to find

$$U_g^0\mathrm{C}_g^0 = 2\alpha\left(1 - e^{-t/\epsilon}\right)\int_{y=0}^{y=z}\left(T(y) - T_m\right)dy, \tag{25}$$

and hence $P^0 = \frac{1}{2}$. We can find C_g^0 from the reduced, leading order no-voids condition

$$g_0\left(T + \frac{T_{\mathrm{top}}}{T_0}\right)\mathrm{C}_g^0 + m_{\mathrm{C}} + m_{\mathrm{SiO_2(s)}}\alpha + \mathcal{O}(\epsilon) = 1, \tag{26}$$

so that for prescribed $T(z)$

$$\mathrm{C}_g^0 = \frac{1 - m_{\mathrm{C}} - m_{\mathrm{SiO_2(s)}}\alpha}{g_0\left(T(z) + \frac{T_{\mathrm{top}}}{T_0}\right)}. \tag{27}$$

Thus the concentration of gas increases as the temperature decreases higher up in the furnace. The leading order gas velocity U_g^0 can then be found using (25) and (27). Note that on an even smaller $\mathcal{O}(\delta)$ timescale different behavior would be found, with the time derivative of $\mathrm{C}_g^0(1 - P^0)$ and $\mathrm{C}_g^0 P^0$ balancing with the convective flux and reaction r_5^0. However, the resulting wave-like behavior only describes the very fast transient behavior of the gas flux and pressure and so is not discussed for the sake of brevity.

Copyright © by SIAM. Unauthorized reproduction of this article is prohibited.

3.2. Region IIb—order one time crater and cavity. We next examine behavior in the outer-in-time crater and cavity region. Here we have the order one timescale t. The order one equations are found to be

$$\frac{\partial \mathrm{C}_{\mathrm{C}}^0}{\partial t} = -r_5^0, \quad \frac{\partial \mathrm{C}_{\mathrm{SiO_2(s)}}^0}{\partial t} = -r_3^0,$$
$$0 = r_3^0 - r_5^0, \quad \frac{\partial}{\partial z}\left(U_g^0 \mathrm{C}_g^0 (1 - P^0)\right) = r_5^0, \quad \frac{\partial}{\partial z}\left(U_g^0 \mathrm{C}_g^0 P^0\right) = r_5^0, \tag{28}$$

which all have $\mathcal{O}(\epsilon)$ corrections, and the no-voids equation is

$$g_0 \left(T + \frac{T_{\mathrm{top}}}{T_0}\right) \mathrm{C}_g^0 + m_{\mathrm{C}} \mathrm{C}_{\mathrm{C}}^0 + m_{\mathrm{SiO_2(s)}} \mathrm{C}_{\mathrm{SiO_2(s)}}^0 = 1 + \mathcal{O}(\epsilon). \tag{29}$$

From the third equation in (28) we have a leading order balance between the melting of quartz r_3^0 and the production of CO and SiO gas from liquid quartz and carbon, r_5^0. This corresponds to a quasi-steady-state assumption, since the time rate of change of liquid quartz is an order smaller than the reaction rates r_3 and r_5. This reaction balance was the motivation for choosing $\epsilon = k_3 T_0 / k_5 c_0$ and scaling the concentrations of SiC, SiO_2(s), and Si to be $\mathcal{O}(\epsilon)$ in section 2. We have the reaction rate $r := r_3^0 = r_5^0$ from this balance and find it is easiest to work with

$$r := \mathrm{C}_{\mathrm{SiO_2(s)}}^0 (T - T_m). \tag{30}$$

As the leading order terms for the concentrations of carbon and solid quartz in Region IIa are the initial conditions, the solutions in Region IIb can be found to be

$$\mathrm{C}_{\mathrm{C}}^0 = \alpha e^{-(T - T_m)t} + (1 - \alpha), \quad \mathrm{C}_{\mathrm{SiO_2(s)}}^0 = \alpha e^{-(T - T_m)t}. \tag{31}$$

In Figure 3 we compare these solutions with the numerical results for a simulation with a fixed temperature profile, showing a good fit. We can find $\mathrm{C}_{\mathrm{SiO_2(l)}}^0$ from the balance between r_3^0 and r_5^0 to give

$$\mathrm{C}_{\mathrm{SiO_2(l)}}^0 = \frac{\mathrm{C}_{\mathrm{SiO_2(s)}}^0 (T - T_m)}{\mathrm{C}_{\mathrm{C}}^0} = \frac{(T - T_m)\alpha e^{-(T - T_m)t}}{\alpha e^{-(T - T_m)t} + (1 - \alpha)}. \tag{32}$$

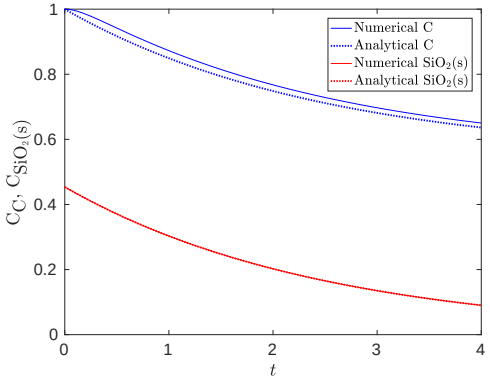

FIG. 3. *Dimensionless concentration of carbon, in blue, and solid quartz, in red, at height* $z = 0.3$. *We compare numerical solutions of the full system with* $T(z)$ *in solid lines to asymptotic solution in dashed lines, with parameter values* $\epsilon = 0.16$, $\delta = 3.2 \times 10^{-4}$, *and* $\alpha = 0.45$.

Downloaded 04/19/18 to 129.67.185.193. Redistribution subject to SIAM license or copyright; see http://www.siam.org/journals/ojsa.php

Copyright © by SIAM. Unauthorized reproduction of this article is prohibited.

Downloaded 04/19/18 to 129.67.185.193. Redistribution subject to SIAM license or copyright; see http://www.siam.org/journals/ojsa.php

Although this tends to zero as t increases, it does not satisfy the initial condition of $\mathrm{C}_{\mathrm{SiO_2(l)}} = 0$. This is accounted for in section 3.1, where the early time behavior was examined.

To find the gas flux we add the last two equations in (28) and integrate spatially, applying the no-flux boundary condition $U_g^0(0,t) = 0$, to give

$$\begin{aligned} U_g^0(z,t)\mathrm{C}_g^0(z,t) &= 2\alpha \int_{y=0}^{y=z} e^{-(T(y)-T_m)t}\left(T(y)-T_m\right) dy \\ &= -2\alpha \frac{\partial}{\partial t} \int_{y=0}^{y=z} e^{-(T(y)-T_m)t} dy. \end{aligned} \tag{33}$$

We can find the leading order pressure by integrating the last equation in (28) and noting

$$U_g^0 \mathrm{C}_g^0 P^0 = \frac{1}{2} U_g^0 C_g^0 + g(t). \tag{34}$$

The arbitrary function of time $g(t)$ is zero from the no-flux boundary condition for velocity, and since $U_g^0 \mathrm{C}_g^0 \neq 0$ in general, we again have $P^0 = \frac{1}{2}$.

We can find the concentration of gas through (29), giving

$$\mathrm{C}_g^0 = \frac{1}{g_0\left(T + \frac{T_{\mathrm{top}}}{T_0}\right)} \left(1 - (m_{\mathrm{C}} + m_{\mathrm{SiO_2(s)}})\alpha e^{-(T-T_m)t} - m_{\mathrm{C}}(1-\alpha)\right). \tag{35}$$

Notice that although this is not a separable solution, we can decompose it as $\mathrm{C}_g^0(z,t) = X(z)Y(t,z)$ for

$$X(z) := \frac{1}{g_0\left(T + \frac{T_{\mathrm{top}}}{T_0}\right)}, \quad Y(t,z) := 1 - (m_{\mathrm{C}} + m_{\mathrm{SiO_2(s)}})\alpha e^{-(T-T_m)t} - m_{\mathrm{C}}(1-\alpha). \tag{36}$$

Thus $Y(0,z) = 1 - m_{\mathrm{SiO_2(s)}}\alpha - m_{\mathrm{C}}$ and $Y(t,z) \to 1 - m_{\mathrm{C}}(1-\alpha)$ as $t \to \infty$. This means that there is a saturation level for the gas concentration, which happens as the concentrations of carbon and solid quartz tend toward their long time behavior.

If required, we could calculate the velocity from the solutions for the gas flux and the gas concentration. For example, using our specific example temperature profile $T(z) = \min(1, \frac{1-z}{1-h_T^*})$, in the region $0 \leq z \leq h_T^*$ where $T(z) \equiv 1$, we have

$$U_g^0(z,t) = 2\alpha \frac{(1-T_m)e^{-(1-T_m)t} z}{\mathrm{C}_g^0(z,t)}. \tag{37}$$

We can find composite asymptotic solutions valid for all time by combining our inner-in-time and outer-in-time solutions. Letting y_I denote an inner solution, y_O an outer solution, and $y_{overlap}$ the overlap, we have that the composite solution y_c is given by $y_c = y_I + y_O - y_{overlap}$. The composite solution for the concentration of $\mathrm{SiO_2(l)}$ is thus

$$\mathrm{C}_{\mathrm{SiO_2(l)}}^0 = \alpha(T - T_m)\left[\frac{e^{-(T-T_m)t}}{\alpha e^{-(T-T_m)t} + (1-\alpha)} - e^{-\frac{t}{\epsilon}}\right]. \tag{38}$$

Similarly for the gas flux we have

$$U_g^0(z,t)\mathrm{C}_g^0(z,t) = 2\alpha \int_{y=0}^{y=z} (T(y) - T_m)\left(e^{-(T(y)-T_m)t} - e^{-\frac{t}{\epsilon}}\right) dy. \tag{39}$$

Copyright © by SIAM. Unauthorized reproduction of this article is prohibited.

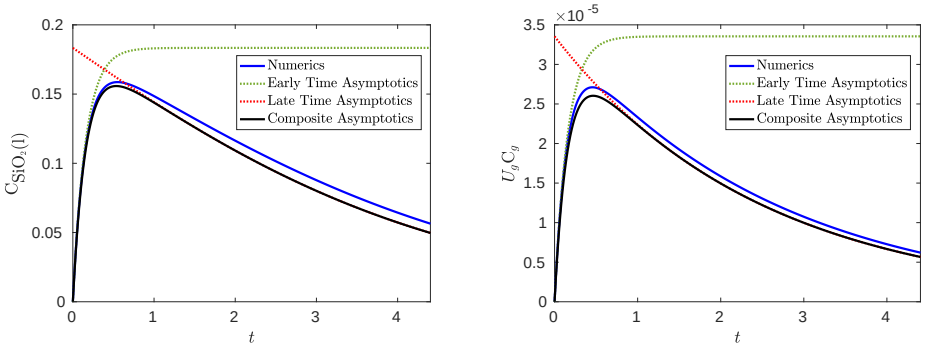

FIG. 4. *Comparison of early time, late time, and composite asymptotics, with numerics of the full system with prescribed temperature profile at height $z = 0.3$. On the left is the concentration of liquid quartz and on the right is the gas flux (both dimensionless). Parameter values used are $\epsilon = 0.16$, $\delta = 3.2 \times 10^{-4}$, $\alpha = 0.45$, $\chi_1 = 0.15$, and $\chi_2 = 0.25$.*

In Figure 4 we compare the early time, late time, and composite asymptotics with numerics for the full system, for the concentration of liquid quartz and the gas flux. The numerical and composite asymptotic curves match in long time, as the variables go to zero. The difference between the curves is due to reactions r_2 and r_{-2}, which do not appear in the leading order asymptotics.

The equations for the leading order concentrations of SiC and Si are

$$\epsilon \frac{\partial C^0_{SiC}}{\partial t} = \epsilon\chi_1 \left(\alpha e^{-(T-T_m)t} + (1-\alpha)\right) \left(\frac{1}{2} - P_1\right)^+ - \epsilon\chi_4 C^0_{SiC} \left(\frac{1}{2} - P_4\right)^+ + \mathcal{O}(\epsilon^2), \tag{40}$$

$$\epsilon \frac{\partial C^0_{Si}}{\partial t} = \epsilon\chi_2 \left(\frac{1}{2} - P_2\right)^+ - \epsilon\chi_{-2} \left(\frac{(T-T_m)\alpha e^{-(T-T_m)t}}{\alpha e^{-(T-T_m)t} + (1-\alpha)}\right) C^0_{Si} + 2\epsilon\chi_4 C^0_{SiC} \left(\frac{1}{2} - P_4\right)^+ + \mathcal{O}(\epsilon^2). \tag{41}$$

These, along with the the zero initial conditions (20), could be solved analytically by first solving (40) and then substituting this into (41). In the typical temperature range found in Region II we find $P_1 < \frac{1}{2}$, but P_2 and P_4 can be smaller or larger than $\frac{1}{2}$, and so the different cases would need to be considered individually. We do not include these cases here.

3.3. Region Ia—early time furnace charge. We now consider the upper region in the furnace, which corresponds to the furnace charge. In this region $T < T_m$ so the solid quartz does not melt, and $r_3 \equiv 0$. Hence $C_{SiO_2(s)} = \alpha$ for all time and we now have seven equations for the remaining seven unknowns, being the concentrations of C, SiC, SiO_2(l), Si, and gas, the partial pressure P, and the gas flux U_g. We begin with Region Ia, where we analyze the early time behavior. Using the same timescale as in Region IIa, $t = \epsilon\hat{t}$, we find the leading order equations for each variable are given by

$$\frac{1}{\epsilon}\frac{\partial C^0_C}{\partial \hat{t}} = \mathcal{O}(1), \quad \frac{\partial C^0_{SiC}}{\partial \hat{t}} = \mathcal{O}(\epsilon), \quad \frac{\partial C^0_{SiO_2(l)}}{\partial \hat{t}} = -r_5^0 + \mathcal{O}(\epsilon), \quad \frac{\partial C^0_{Si}}{\partial \hat{t}} = \mathcal{O}(\epsilon), \tag{42}$$

$$\frac{\partial}{\partial z}\left(U_g^0 C_g^0 (1 - P^0)\right) = r_5^0 + \mathcal{O}(\epsilon), \quad \frac{\partial}{\partial z}\left(U_g^0 C_g^0 P^0\right) = r_5^0 + \mathcal{O}(\epsilon), \tag{43}$$

$$g_0 \left(T + \frac{T_{top}}{T_0}\right) C_g^0 + m_C C_C^0 + m_{SiO_2(s)}\alpha = 1 + \mathcal{O}(\epsilon). \tag{44}$$

Copyright © by SIAM. Unauthorized reproduction of this article is prohibited.

Downloaded 04/19/18 to 129.67.185.193. Redistribution subject to SIAM license or copyright; see http://www.siam.org/journals/ojsa.php

Downloaded 04/19/18 to 129.67.185.193. Redistribution subject to SIAM license or copyright; see http://www.siam.org/journals/ojsa.php

Clearly $\mathrm{C}_{\mathrm{C}}^0 = 1$, $\mathrm{C}_{\mathrm{SiC}}^0 = 0$, and $\mathrm{C}_{\mathrm{Si}}^0 = 0$. Since $r_5^0 = \mathrm{C}_{\mathrm{C}}^0 \mathrm{C}_{\mathrm{SiO_2(l)}}^0 = \mathrm{C}_{\mathrm{SiO_2(l)}}^0$ we find the third equation in (42) leads to $\mathrm{C}_{\mathrm{SiO_2(l)}}^0 = 0$, since the preexponential factor is zero from the initial condition. Thus the leading order concentrations of the solid and liquid species are given by their initial conditions, and they do not alter significantly in the early time. When analyzing their dynamics in Region Ib we will use initial conditions for the whole model (20). Similarly, since $\mathrm{C}_{\mathrm{C}}^0 = 1$ and $\mathrm{C}_{\mathrm{SiO_2(s)}}^0 = \alpha$, C_g^0 is constant, given by (44). We then find that $U_g^0 \mathrm{C}_g^0$ and P^0 are both functions of time only, since $r_5^0 = 0$. We can find these functions by imposing continuity of the gas flux and pressure across the interface $z = z_m$ (which is $z : T(z) = T_m$) and utilizing solutions from Region IIa below. Hence $P^0 = \frac{1}{2}$ and

$$U_g^0 \mathrm{C}_g^0 = 2\alpha \left(1 - e^{-t/\epsilon}\right) \int_{y=0}^{y=z_m} (T(y) - T_m)\, dy, \tag{45}$$

where we have used the gas flux at $z = z_m$ from (25).

3.4. Region Ib—order one time furnace charge. We now consider order one time behavior in the upper furnace, where $T < T_m$. We find the leading order equations for the solid and liquid concentrations are

$$\begin{aligned} &\frac{\partial \mathrm{C}_{\mathrm{C}}^0}{\partial t} = -r_5^0 + \mathcal{O}(\epsilon), \quad \epsilon \frac{\partial \mathrm{C}_{\mathrm{SiC}}^0}{\partial t} = \epsilon r_1^0 - \epsilon r_4^0 + \mathcal{O}(\epsilon^2), \quad 0 = -r_5^0 + \mathcal{O}(\epsilon), \\ &\epsilon \frac{\partial \mathrm{C}_{\mathrm{Si}}^0}{\partial t} = \epsilon r_2^0 - \epsilon r_{-2}^0 + \epsilon r_4^0 + \mathcal{O}(\epsilon^2), \end{aligned} \tag{46}$$

along with the gas flux equations (43) and the reduced no-voids equation (44) from Region Ia. Since $r_5^0 = 0$, then $\mathrm{C}_{\mathrm{C}}^0 = 1$ and the partial pressure and gas flux are again given by imposing continuity from below, this time with Region IIb, to give $P^0 = \frac{1}{2}$, and

$$U_g^0 \mathrm{C}_g^0 = 2\alpha \int_{y=0}^{y=z_m} e^{-(T(y)-T_m)t}\, (T(y) - T_m)\, dy, \tag{47}$$

using (33). Also, since $r_5^0 = 0$ and $r_5^0 = \mathrm{C}_{\mathrm{C}}^0 \mathrm{C}_{\mathrm{SiO_2(l)}}^0$, then $\mathrm{C}_{\mathrm{SiO_2(l)}}^0 = 0$, and hence $r_{-2}^0 = \chi_{-2} \mathrm{C}_{\mathrm{SiO_2(l)}}^0 \mathrm{C}_{\mathrm{Si}}^0 = 0$. We now examine the $\mathcal{O}(\epsilon)$ equations for the concentrations of solid and liquid species,

$$\begin{aligned} &\frac{\partial \mathrm{C}_{\mathrm{C}}^1}{\partial t} = -2r_1^0 - r_5^1 + \mathcal{O}(\epsilon), \quad \frac{\partial \mathrm{C}_{\mathrm{SiC}}^0}{\partial t} = r_1^0 - r_4^0 + \mathcal{O}(\epsilon), \quad 0 = r_2^0 - r_5^1 + \mathcal{O}(\epsilon), \\ &\frac{\partial \mathrm{C}_{\mathrm{Si}}^0}{\partial t} = r_2^0 + 2r_4^0 + \mathcal{O}(\epsilon). \end{aligned} \tag{48}$$

There is a balance between r_2 and r_5, so that the liquid quartz, which condenses through r_2, reacts with the available carbon through r_5. Since reaction r_5 is limited by the amount of liquid quartz available, it is $\mathcal{O}(\epsilon)$ in the upper furnace, which is much smaller than the $\mathcal{O}(1)$ reaction in the lower furnace, in which the available liquid quartz is provided through reaction r_3, the melting of solid quartz. Indeed, to order one no reactions take place in the furnace charge and the chemical species remain in their initial state. To find the $\mathcal{O}(\epsilon)$ changes to the chemical species we utilize the balance $r_2^0 = r_5^1$ and solutions $\mathrm{C}_{\mathrm{C}}^0 = 1$ and $P^0 = \frac{1}{2}$. In addition, when $T < T_m$ we have that $P_4 > \frac{1}{2}$, but $P_1, P_2 < \frac{1}{2}$ (see the equilibrium partial pressure diagram in [17]). Hence, we have that

Copyright © by SIAM. Unauthorized reproduction of this article is prohibited.

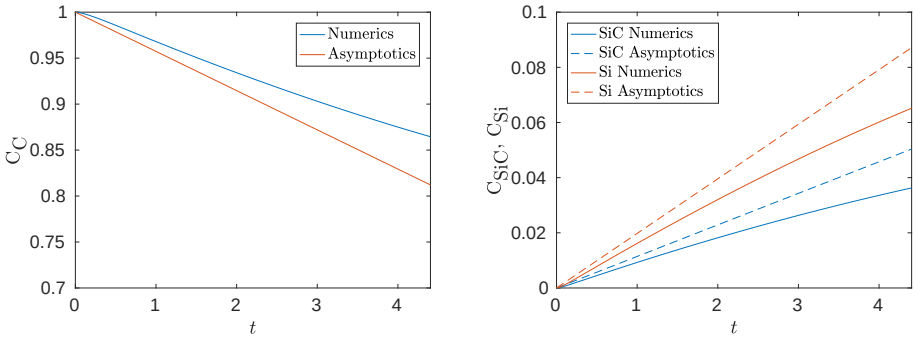

FIG. 5. *Comparison of numerics and asymptotics at $z = 0.9$. On the left are plots of the dimensionless concentration of carbon, showing numerics in blue and asympotics in red. On the right are plots of the dimensionless concentrations of SiC (in blue) and Si (in red), showing numerics in solid and asympotics in dashed. There is agreement to $\mathcal{O}(\epsilon)$ but noticeable $\mathcal{O}(\epsilon^2)$ disagreement, which would be reduced by considering more terms. Notice that the scale for the left plot is between 0.7 and 1, so there is an approximate 5% error for C_C, and the scale on the right plot is only up to 0.1, so the absolute error for C_{SiC} and C_{Si} is also small, since these are order one dimensionless variables. Parameter values used are $\epsilon = 0.16$, $\delta = 3.2 \times 10^{-4}$, $\chi_1 = 0.15$, and $\chi_2 = 0.25$.*

$$(49)\quad \frac{\partial \mathrm{C}_{\mathrm{C}}^1}{\partial t} = -2\chi_1\left(\frac{1}{2} - P_1\right) - \chi_2\left(\frac{1}{2} - P_2\right),\ \frac{\partial \mathrm{C}_{\mathrm{SiC}}^0}{\partial t} = \chi_1\left(\frac{1}{2} - P_1\right),\ \frac{\partial \mathrm{C}_{\mathrm{Si}}^0}{\partial t} = \chi_2\left(\frac{1}{2} - P_2\right).$$

In section 3.3 we calculated $\mathrm{C_C}$ only to first order, but we can easily find that in Region Ia $\mathrm{C}_{\mathrm{C}}^1 = 0$. Hence we can use the zero Dirichlet condition for $\mathrm{C}_{\mathrm{C}}^1$ in Region Ib, as well as for $\mathrm{C}_{\mathrm{SiC}}^0$ and $\mathrm{C}_{\mathrm{Si}}^0$, to find

$$(50)\quad \mathrm{C}_{\mathrm{C}}^1 = -\left(2\chi_1\left(\frac{1}{2} - P_1\right) + \chi_2\left(\frac{1}{2} - P_2\right)\right)t,\ \mathrm{C}_{\mathrm{SiC}}^0 = \chi_1\left(\frac{1}{2} - P_1\right)t,\ \mathrm{C}_{\mathrm{Si}}^0 = \chi_2\left(\frac{1}{2} - P_2\right)t.$$

We show comparisons of these solutions with numerics in Figure 5. We have that carbon is being lost to gas through reaction r_5 (reacting with the liquid quartz produced through r_2) and to silicon carbide through reaction r_1. The production of silicon through r_2 is equal to the loss of carbon through r_5, since all the available liquid quartz reacts with carbon (to leading order). The dynamics in the furnace charge are driven by the behavior of convecting SiO molecules, which can condense through r_2, leading to silicon production, react with carbon, through r_1 to produce silicon carbide, or convect out of the furnace unreacted. The parameter $\lambda = \chi_2/\chi_1$ determines the relative importance of reactions r_1 and r_2. The higher λ is, the more silicon will be produced. The lower λ is, the more silicon carbide will build up.

We now find the $\mathcal{O}(\epsilon)$ corrections to the gas flux and the pressure. Adding the last two rows in (14) gives an equation for the gas flux, which we treat as one variable (so that $U_g \mathrm{C}_g = U_g^0 \mathrm{C}_g^0 + \epsilon U_g^1 \mathrm{C}_g^1 + \mathcal{O}(\epsilon^2)$). We have that $U_g^0 \mathrm{C}_g^0 = f(t)$, given by (47), and find that

$$(51)\qquad \epsilon \frac{\partial}{\partial z}\left(U_g^1 \mathrm{C}_g^1\right) = -2\epsilon r_2^0 + 2\epsilon r_5^1 + \mathcal{O}(\epsilon^2).$$

By the balance $r_2^0 = r_5^1$ in (48) we have that $U_g^1 \mathrm{C}_g^1$ is also a function of time only, which could be given from matching with the region below, Region IIb, if we desired. The $\mathcal{O}(\epsilon)$ equation for P^1 is

Copyright © by SIAM. Unauthorized reproduction of this article is prohibited.

Downloaded 04/19/18 to 129.67.185.193. Redistribution subject to SIAM license or copyright; see http://www.siam.org/journals/ojsa.php

$$\epsilon \frac{\partial}{\partial z}\left(U_g^0 \mathrm{C}_g^0 P^1 + U_g^1 \mathrm{C}_g^1 P^0\right) = -\epsilon r_1^0 - 2\epsilon r_2^0 + \epsilon r_5^1 + \mathcal{O}(\epsilon^2), \tag{52}$$

where we have noted that $r_{-2}^0 = r_4^0 = 0$. Using $r_5^1 = r_2^0$, and since $U_g^0 \mathrm{C}_g^0 = f(t)$ and $U_g^1 \mathrm{C}_g^1 P^0$ are both spatially independent, we have

$$f(t)\frac{\partial P^1}{\partial z} = -\left(\chi_1\left(\frac{1}{2} - P_1(T(z))\right) + \chi_2\left(\frac{1}{2} - P_2(T(z))\right)\right). \tag{53}$$

This implies

$$P^1 = \frac{A(z)}{f(t)} + b(t), \tag{54}$$

where $A(z)$ is a decreasing function in z and $b(t)$ is an arbitrary function of time. Since $f(t) \to 0$ as $t \to \infty$ this form of P^1 breaks down after a long time. The timescale on which $P^1 = \mathcal{O}(\epsilon^{-1})$, thus breaking down the asymptotic expansion, is the timescale on which $f(t) = U_g^0 \mathrm{C}_g^0$ given by (47) is $\mathcal{O}(\epsilon)$ (assuming $A(z) = \mathcal{O}(1)$). Assuming $M/2\alpha := \max|T'(y)|$ is an order one constant and letting $x := T(y) - T_m$, we have

$$|f(t)| \leq M\left|\int_{x=0}^{1-T_m} x e^{-xt} dx\right| \leq M t^{-2}, \tag{55}$$

and so this happens for $t = \mathcal{O}(\epsilon^{-1/2})$. In numerical simulations we find that $P \to P_2$ in long time behavior, so that the condensation of SiO stops, but the reaction r_1 with carbon continues (as $P_2 > P_1$ [17]).

By prescribing a temperature profile $T(z)$ we have identified two spatial regions—a lower crater and cavity region, in which there is a balance between reactions r_3 and r_5, and an upper furnace charge region, in which chemical changes occur in smaller $\mathcal{O}(\epsilon)$ quantities and there is a balance between reactions r_2 and r_5. By expanding variables in terms of the small parameter ϵ we have found analytic solutions throughout the furnace, with composite solutions for early time and order one time behavior in Region II where appropriate. Information propagates upward from the crater and cavity to the charge through the gas flux—an effect that we have quantified. In the charge there is competition between reactions r_1, producing SiC, and r_2, producing Si.

4. Full model asymptotics. We now consider asymptotics of the full model, comprising (14)–(16), initial conditions (20), and boundary conditions (11). We utilize the balances developed in section 3 and extend our analysis to consider a spatially and temporally varying temperature $T(z,t)$. In the pilot furnace experiments we see that the interface between the furnace charge and the cavity region rises as the furnace heats up. We would thus expect to have regions similar to Regions I and II as in Figure 2, except that the interface $z = z_m$ moves with time. Considering the full model with varying temperature is thus important, because it captures this rising interface. In this section we reduce our model to two coupled equations for temperature and the concentration of solid quartz, which are dependent on three parameters. This simplified coupled model captures much of the qualitative behavior of the full model, which has 9 variables and over 30 parameters. We analyze early time behavior, before reactions occur significantly, and consider the limit of small diffusion. We also comment on the joint limits of small diffusion and small external heating.

We consider leading order terms in the conservation of energy equation (16) in the limit $\epsilon \to 0$ and $\delta/\epsilon \to 0$. The superscript notation ^{0} used in section 3 is dropped, with the assumption that all variables used to determine the simplified system are $\mathcal{O}(1)$.

Copyright © by SIAM. Unauthorized reproduction of this article is prohibited.

Downloaded 04/19/18 to 129.67.185.193. Redistribution subject to SIAM license or copyright; see http://www.siam.org/journals/ojsa.php

Downloaded 04/19/18 to 129.67.185.193. Redistribution subject to SIAM license or copyright; see http://www.siam.org/journals/ojsa.php

Although there are different equations in Regions I and II in section 3, the changes in Region II are of higher order than in the other regions, so our leading order equations capture these effects primarily. To $\mathcal{O}(1)$ no chemical changes occur in the top of the furnace, but reactions and chemical transformations happen in the base. There is a balance between reactions r_3 and r_5 in the furnace base, so we integrate the first two equations in (28) to get the algebraic relation $\mathrm{C_C} = \mathrm{C_{SiO_2(s)}} + (1-\alpha)$. Note that this does not hold in the top of the furnace, where carbon slowly decays but the concentration of solid quartz remains constant. However, this is an $\mathcal{O}(\epsilon)$ effect only. Noting that to leading order $P = \frac{1}{2}$, we then have

(56)
$$\sigma_s = \mathrm{C_{SiO_2(s)}}\left(1+C_{P,\mathrm{SiO_2(s)/C}}\right)+(1-\alpha)+\mathcal{O}(\epsilon),\ \sigma_g=\frac{1}{2}\mathrm{C}_g\left(C_{P,\mathrm{CO/C}}+C_{P,\mathrm{SiO/C}}\right)+\mathcal{O}(\epsilon)$$

as leading order terms to (18) and (19). Combining these with the leading order terms in (16), and using $r = \mathrm{C_{SiO_2(s)}}(T-T_m)^+$ as the functional form for $r := r_3 = r_5$, we obtain the leading order equations, with $\mathcal{O}(\epsilon)$ corrections,

$$\begin{aligned}&\frac{\partial}{\partial t}\left(\left(\frac{T_{top}}{T_0}+T\right)\left(\sigma_s+\sigma^*_{gr}\right)\right)+\frac{\partial}{\partial z}\left(\left(\frac{T_{top}}{T_0}+T\right)\frac{U_g\sigma_g}{2}\right)\\ &\quad = a\frac{\partial T^2}{\partial z^2}+\beta^*\frac{\partial}{\partial z}\left(\left(\frac{T_{top}}{T_0}+T\right)^3\frac{\partial T}{\partial z}\right)+\gamma_5\mathrm{C_{SiO_2(s)}}(T-T_m)^+ + qF(z),\end{aligned} \tag{57}$$

$$\frac{\partial}{\partial z}\left(U_g\mathrm{C}_g\right) = 2\mathrm{C_{SiO_2(s)}}(T-T_m)^+,\quad \frac{\partial \mathrm{C_{SiO_2(s)}}}{\partial t} = -\mathrm{C_{SiO_2(s)}}(T-T_m)^+, \tag{58}$$

$$g_0\left(T+\frac{T_{\mathrm{top}}}{T_0}\right)\mathrm{C}_g + \mathrm{C_{SiO_2(s)}}(m_{\mathrm{C}}+m_{\mathrm{SiO_2(s)}})+(1-\alpha)m_{\mathrm{C}} = 1, \tag{59}$$

along with boundary and initial conditions

(60)
$$\frac{\partial T(0,t)}{\partial z} = 0 = \frac{\partial T(1,t)}{\partial z},\ T(z,0) = T_a = -1.1,\ U_g(0,t) = 0,\ \mathrm{C_{SiO_2(s)}}(z,0) = \alpha.$$

We further simplify our system by neglecting radiation, since $\beta^*(\frac{T_{top}}{T_0}+T)^3/a \sim 0.27$ at the base, and thermal convection from (57). Although these are both order one effects, we seek to get the simplest model which represents the main physical and chemical effects, thus making the analysis more tractable. We thus replace (57) with

$$\begin{aligned}&\frac{\partial}{\partial t}\left(\left(\frac{T_{top}}{T_0}+T\right)\left(\mathrm{C_{SiO_2(s)}}\left(1+C_{P,\mathrm{SiO_2(s)/C}}\right)+(1-\alpha)+\sigma^*_{gr}\right)\right)\\ &\quad = a\frac{\partial T^2}{\partial z^2}+\gamma_5\mathrm{C_{SiO_2(s)}}(T-T_m)^+ + qF(z).\end{aligned} \tag{61}$$

The gas flux equation, which is the first in (58), decouples and we are left with the system (61) and the second equation in (58) to be solved for the temperature and concentration of solid quartz. This is still quite complex, so we make an additional approximation. Since the model assumes a constant thermal conductivity, it is not unreasonable to replace the varying heat capacity with a constant heat capacity. We take this to be the average of the minimum and maximum values of the heat capacity, that is,

Copyright © by SIAM. Unauthorized reproduction of this article is prohibited.

$$\sigma = \frac{\alpha}{2}\left(1 + C_{P,\mathrm{SiO_2(s)/C}}\right) + (1-\alpha) + \sigma^*_{gr}. \tag{62}$$

We note that γ_5 is negative [20], so for clarity we use the notation $\gamma := -\gamma_5$. This give the system

$$\sigma\frac{\partial T}{\partial t} = a\frac{\partial T^2}{\partial z^2} - \gamma \mathrm{C_{SiO_2(s)}}(T-T_m)^+ + qF(z), \quad \frac{\partial \mathrm{C_{SiO_2(s)}}}{\partial t} = -\mathrm{C_{SiO_2(s)}}(T-T_m)^+, \tag{63}$$

$$\frac{\partial T(0,t)}{\partial z} = 0 = \frac{\partial T(1,t)}{\partial z}, \quad T(z,0) = T_a = -1.1, \quad \mathrm{C_{SiO_2(s)}}(z,0) = \alpha. \tag{64}$$

We have the furnace heating up from cold due to a wall source term $F(z)$, up to a time when the temperature reaches the melting point of quartz, T_m, in the base of the furnace. Then solid quartz melts to form liquid quartz, at a rate $r_3 = \mathrm{C_{SiO_2(s)}}(T - T_m)^+$. This melting does not release any heat in our full model, but we have a reaction balance between the reactions r_3 and r_5, in which carbon reacts with the newly formed liquid quartz to produce gaseous CO and SiO. This pair of reactions is highly endothermic, taking in heat from the surroundings. Thus, energy needs to be input from the walls in order for the carbon and quartz to react, but since this reaction is endothermic it slows down the rate of temperature increase.

In order to write this system in a cleaner mathematical form, we choose to rescale time to balance with the endothermic heat of reaction, so we introduce the scalings

$$T = T_m + \hat{T}(T_m - T_a), \quad \mathrm{C_{SiO_2(s)}} = \alpha\hat{C}, \quad t = \frac{\sigma}{\gamma\alpha}\hat{t}. \tag{65}$$

Dropping the hat notation we have the system

$$\frac{\partial T}{\partial t} = K\frac{\partial^2 T}{\partial z^2} - CT^+ + \omega F(z), \tag{66}$$

$$\frac{\partial C}{\partial t} = -bCT^+, \tag{67}$$

with initial and boundary conditions

$$T(z,0) = -1, \quad C(z,0) = 1, \quad \frac{\partial T(0,t)}{\partial z} = 0 = \frac{\partial T(1,t)}{\partial z}. \tag{68}$$

The three dimensionless parameters are written in terms of previous dimensionless parameters as

$$K = \frac{a}{\gamma\alpha}, \quad b = \frac{(T^*_m - T_a)\sigma}{\gamma\alpha}, \quad \omega = \frac{q}{(T^*_m - T_a)\gamma\alpha}. \tag{69}$$

Typical parameter sizes are $K = 0.01$, $b = 0.3$, and $\omega = 0.15$. We will use these values throughout this section unless otherwise stated. In Figure 6 we show plots comparing the numerical solutions of this simplified system with the full system presented in section 1. In the full system heat equation (16) the heat capacity can vary, so for a fair comparison we restrict the heat capacity in the time derivative of the full numerics to be the constant σ from (62). We could alternatively have kept a varying heat capacity in the simplified system, but this would make the asymptotic analysis more difficult. The heat capacity of the gas in the spatial derivative of (16) is still allowed to vary, since this is not included in the simplified model. The temperatures of the two systems match well for the first 40 min in the base of the furnace, but the simplified numerics become hotter in the base after this. This is because thermal convection and radiation, which transfer heat from the base to the

Downloaded 04/19/18 to 129.67.185.193. Redistribution subject to SIAM license or copyright; see http://www.siam.org/journals/ojsa.php

Copyright © by SIAM. Unauthorized reproduction of this article is prohibited.

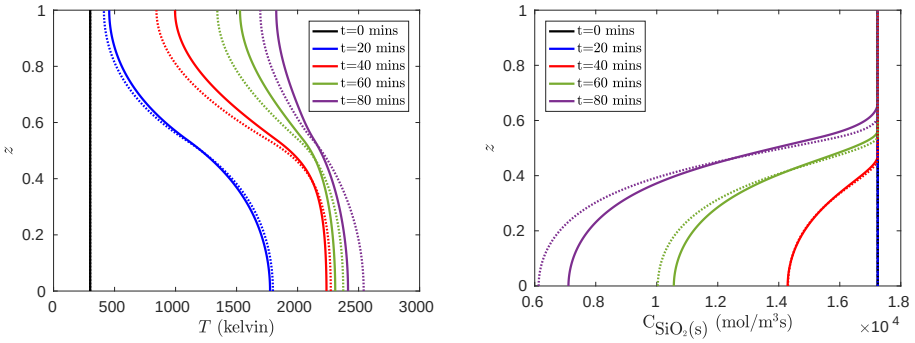

FIG. 6. *Comparison of numerics of the full system* (11), (14)–(20) *(with a constant heat capacity) in solid lines and numerics for the simplified system* (66)–(68) *in dotted lines. On the left are plots of temperature and on the rights are plots of* $C_{SiO_2(s)}$ *(both dimensional). Parameter values used are* $\epsilon = 0.16$, $\delta = 3.2 \times 10^{-4}$, *and* $\alpha = 0.45$.

top of the furnace, are present in the full model but not in the simplified model. The effect of this is to produce more SiO_2(s) in the base in the simplified model. Also, the exothermic heat sources from reactions r_1 and r_2 are present in the full model only, adding to the discrepancy of the temperature in the upper furnace. However, despite these differences, the overall qualitative behavior is similar between the two models. We have the base of the furnace heating up faster than the top and, upon reaching a critical temperature, solid quartz melting then reacting to form gas. It is thus instructive to consider this simplified model to develop understanding as to the qualitative effects in the pilot furnace.

4.1. Early time. For early time the temperature is not hot enough for the reaction to take place, meaning no energy is consumed by the reaction. Taking the heat source from the wall to be the step function $F(z) = \mathcal{H}(h_T^* - z)$ in this case, for ease of analysis, we have

$$\frac{\partial T}{\partial t} = K\frac{\partial^2 T}{\partial z^2} + \omega \mathcal{H}(h_T^* - z), \tag{70}$$

with initial condition and boundary conditions

$$T(z,0) = -1, \quad \frac{\partial T(0,t)}{\partial z} = \frac{\partial T(1,t)}{\partial z} = 0. \tag{71}$$

We can find a series solution to this problem as

$$T(z,t) = T_a + \omega h_T^* t + \frac{2\omega}{K}\sum_{n=1}^{\infty} \frac{\sin(n\pi h_T^*)}{n^3\pi^3}\left(1 - \exp(-Kn^2\pi^2 t)\right)\cos(n\pi z). \tag{72}$$

In Figure 7 we compare this solution to numerics of the system (66)–(68). There is good agreement in the early time preheating region, then the solutions diverge when $T > 0$, where the endothermic reaction occurs.

4.2. Small diffusion limit. In Figure 8 we show contour plots for T and C for the cases $K = 0.01$ and $K = 0$, with $b = 0.3$ and $\omega = 0.15$ in each case. When there is no diffusion, so $K = 0$, we see a sharp interface between a preheating region in the upper left of the (z,t)-plane and a reaction zone in the lower right of the

Copyright © by SIAM. Unauthorized reproduction of this article is prohibited.

Downloaded 04/19/18 to 129.67.185.193. Redistribution subject to SIAM license or copyright; see http://www.siam.org/journals/ojsa.php

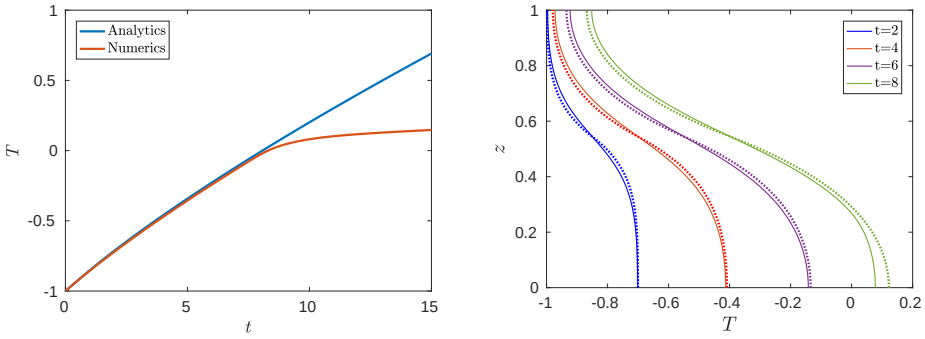

FIG. 7. *Comparison of analytical solution* (72) *with numerics. On the left is the dimensionless temperature for fixed height* $z = 0.3$ *and on the right are spatial profiles at different times, with the analytic solution in dotted lines and numerics in solid lines.*

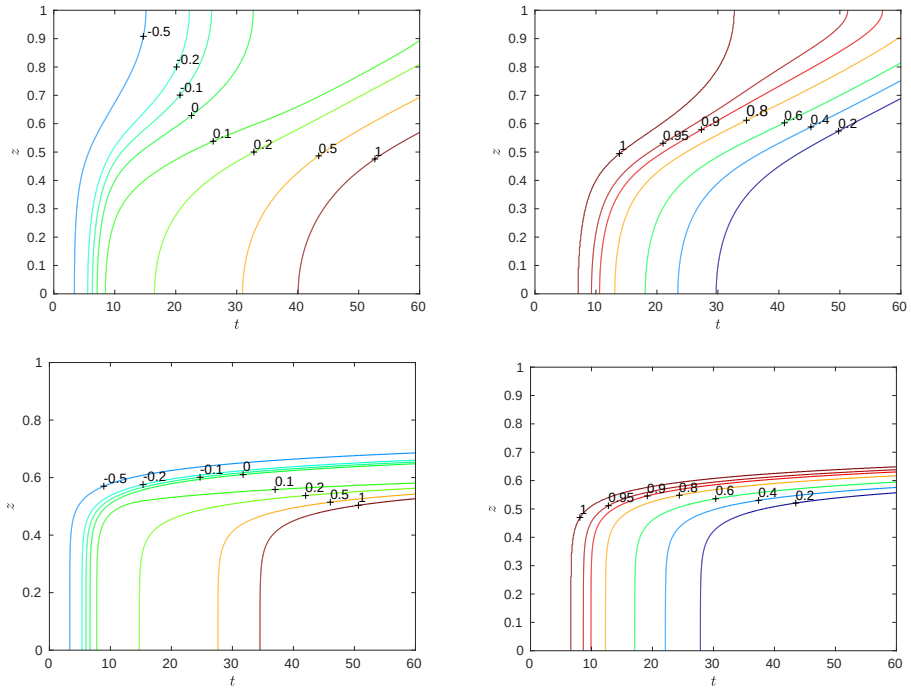

FIG. 8. *Contour plots for dimensionless* T *(left) and* C *(right), in the cases* $K = 0.01$ *(top) and* $K = 0$ *(bottom), with* $b = 0.3$ *and* $\omega = 0.15$ *in all cases.*

plane. Throughout this section and section 4.3 we use the smooth heating function $F(z) = \frac{1}{2}(1 + \tanh(10(h_T^* - z)))$, with $h_T^* = 0.544$, in numerical simulations and asymptotic solutions shown in figures.

A schematic of the two regions is given in Figure 9. Region A is the preheating region, where the temperature is too cold for the reaction to take place. In Region B the temperature is positive, so the chemical reacts. Let $z = s(t)$ be defined as the interface between these regions. We plot numerical solutions for a fixed height $z = 0.3$ in Figure 10, indicating where these regions occur. A third region, Region C, occurs

Copyright © by SIAM. Unauthorized reproduction of this article is prohibited.

Downloaded 04/19/18 to 129.67.185.193. Redistribution subject to SIAM license or copyright; see http://www.siam.org/journals/ojsa.php

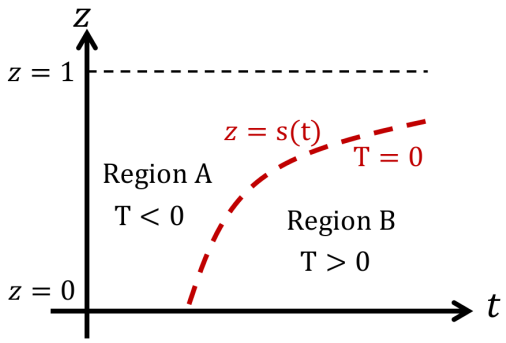

FIG. 9. *Schematic of the different regions in the variable temperature problem. In Region* A *the temperature is too cold for the reaction to take place, while in Region* B *the chemical reacts. These regions are separated by the interface* $z = s(t)$*, given by the isotherm* $T = 0$.

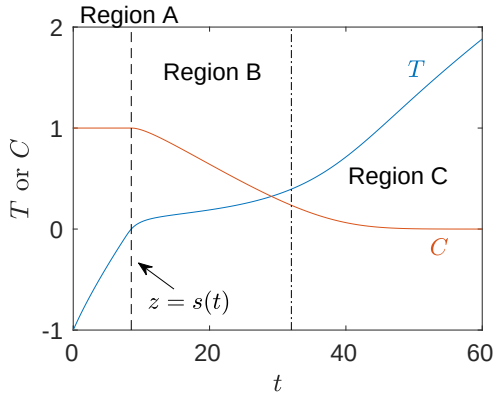

FIG. 10. *Numerical simulations of dimensionless* T *and* C *from the system* (66)–(68)*, displayed for fixed height* $z = 0.3$*. Region* A *is to the left of the dashed line, Region* B *is between the dashed and the dot-dashed lines, and Region* C *is to the right of the dot-dashed line. The dashed line has label* $z = s(t)$*, because it is showing the time for which there is a transition between Regions* A *and* B *for the given height* $z = 0.3$*. The dot-dashed line is in a possible, illustrative location. Parameter values used are* $K = 0.01$*,* $\omega = 0.15$*, and* $b = 0.3$.

where all the chemical is nearly used up and the temperature increases linearly in the graphite crucible due to the heat source from the wall. We are not interested in Region C in this paper, since it corresponds to all the solid material being used up in the furnace, and the pilot furnace experiments do not run for long enough for this to be observed. Unlike the sharp interface between Regions A and B at $z = s(t)$ (shown by the dashed line), there is no sharp interface between Regions B and C; however, we have put an interface in (shown by the dot-dashed line) to illustrate a possible location to distinguish between the regions.

Our model has the small parameter K. We treat ω and b as order one constants and expand in terms of K, with $0 < K \ll 1$, so that we write $T^{A/B} = T_0^{A/B} + KT_1^{A/B} + \mathcal{O}(K^2)$, $C^{A/B} = C_0^{A/B} + KC_1^{A/B} + \mathcal{O}(K^2)$, and $s(t) = s_0(t) + Ks_1(t) + \mathcal{O}(K^2)$, where $T^{A/B}$ and $C^{A/B}$ refer to T and C in Regions A and B, respectively. The first order equations correspond to the limit of zero diffusion. In this case, the spatial dependency for the problem comes through the general heating source term $F(z)$, which we take to be order one and hotter at the base than at the top.

Copyright © by SIAM. Unauthorized reproduction of this article is prohibited.

Downloaded 04/19/18 to 129.67.185.193. Redistribution subject to SIAM license or copyright; see http://www.siam.org/journals/ojsa.php

Downloaded 04/19/18 to 129.67.185.193. Redistribution subject to SIAM license or copyright; see http://www.siam.org/journals/ojsa.php

In Region A we have the system at leading order

$$\frac{\partial T_0^A}{\partial t} = \omega F(z) + \mathcal{O}(K),\ \frac{\partial C_0^A}{\partial t} = \mathcal{O}(K),\ T_0^A(z,0) = -1 + \mathcal{O}(K),\ C_0^A(z,0) = 1 + \mathcal{O}(K), \tag{73}$$

which has the solution

$$T_0^A(z,t) = -1 + \omega F(z)t, \quad C_0^A(z,t) = 1. \tag{74}$$

We find that $C^A \equiv 1$ and that the higher order equations for temperature are given by

$$\frac{\partial T_n^A}{\partial t} = \frac{\partial^2 T_{n-1}^A}{\partial z^2}, \quad n \geq 1. \tag{75}$$

Thus we have the following expansion in K for temperature in Region A:

$$T^A(z,t) = -1 + \omega F(z)t + \omega \sum_{n=1}^{\infty} K^n F^{(2n)}(z) \frac{t^{n+1}}{(n+1)!}. \tag{76}$$

To find the coefficients in the expansion of $s(t)$ we note that the curve $z = s(t)$ is given by

$$T^A(s(t),t) = 0. \tag{77}$$

Hence

$$\begin{aligned} 0 &= T^A(s_0(t) + Ks_1(t) + \ldots, t) \\ &= T^A(s_0(t),t) + (Ks_1(t) + \cdots)\frac{\partial T^A}{\partial z}(s_0(t),t) + \cdots \\ &= T_0^A(s_0(t),t) + K\left(T_1^A(s_0(t),t) + s_1(t)\frac{\partial T_0^A}{\partial z}(s_0(t),t)\right) \\ &\quad + K^2\left(T_2^A(s_0(t),t) + s_1(t)\frac{\partial T_1^A}{\partial z}(s_0(t),t) + s_2(t)\frac{\partial T_0^A}{\partial z}(s_0(t),t)\right. \\ &\qquad \left. + \frac{1}{2}s_1(t)^2\frac{\partial^2 T_0^A}{\partial z^2}(s_0(t),t)\right) + \mathcal{O}(K^3). \end{aligned} \tag{78}$$

Looking at leading order we get

$$\mathcal{O}(1): \quad s_0(t) = F^{-1}\left(\frac{1}{\omega t}\right), \tag{79}$$

which requires that F be invertible. At next order we get

$$\mathcal{O}(K): \quad s_1(t) = -\frac{1}{2}\frac{F''(s_0(t))}{F'(s_0(t))}t, \tag{80}$$

and then looking at terms quadratic in K we find

$$\mathcal{O}(K^2): \quad s_2(t) = \left(\frac{F''(s_0(t))F'''(s_0(t))}{4(F'(s_0(t)))^2} - \frac{F^{IV}(s_0(t))}{6F'(s_0(t))} - \frac{(F''(s_0(t)))^3}{8(F'(s_0(t)))^3}\right)t^2. \tag{81}$$

This iterative process can be continued to find the correction for $s(t)$ to any order of K, if desired.

Copyright © by SIAM. Unauthorized reproduction of this article is prohibited.

Downloaded 04/19/18 to 129.67.185.193. Redistribution subject to SIAM license or copyright; see http://www.siam.org/journals/ojsa.php

In Region B we have obtained the leading order equations,

$$\frac{\partial T_0^B}{\partial t} = -C_0^B T_0^B + \omega F(z) + \mathcal{O}(K), \quad \frac{\partial C_0^B}{\partial t} = -bC_0^B T_0^B + \mathcal{O}(K), \tag{82}$$

with the boundary conditions

$$T_0^B(s_0(t),t) = \mathcal{O}(K), \quad C_0^B(s_0(t),t) = 1 + \mathcal{O}(K), \tag{83}$$

which we can write as

$$T_0^B = 0 \quad \text{and} \quad C_0^B = 1 \quad \text{on} \quad t = \frac{1}{\omega F(z)}. \tag{84}$$

We can write the equations in (82) as

$$\frac{\partial}{\partial t}\left(T_0^B - \frac{1}{b}C_0^B\right) = \omega F(z), \quad \frac{\partial C_0^B}{\partial t} = -bC_0^B T_0^B. \tag{85}$$

Integrating the first equation we get the relation

$$T_0^B = \frac{1}{b}(C_0^B - 1) - 1 + \omega F(z)t, \tag{86}$$

which can be substituted into the second equation to get the ODE

$$\frac{\partial C_0^B}{\partial t} = -(C_0^B)^2 + C_0^B\left(1 + b - b\omega F(z)t\right). \tag{87}$$

Equation (87), along with the boundary condition in (84), has the solution

$$C_0^B(z,t) = \frac{\exp\left(-\frac{2+b}{2\omega F(z)} + (b+1)\,t - \frac{b\omega F(z)}{2}t^2\right)}{1 + \sqrt{\frac{\pi}{2b\omega F(z)}}\exp\left(\frac{1}{2b\omega F(z)}\right)\left[\operatorname{erf}\left(\frac{1}{\sqrt{2b\omega F(z)}}\right) + \operatorname{erf}\left(\frac{b\omega F(z)t - b - 1}{\sqrt{2b\omega F(z)}}\right)\right]}, \tag{88}$$

and hence the temperature is given by

$$T_0^B(z,t) = -1 - \frac{1}{b} + \omega F(z)t + \frac{\exp\left(-\frac{2+b}{2\omega F(z)} + (b+1)\,t - \frac{b\omega F(z)}{2}t^2\right)}{b + \sqrt{\frac{\pi b}{2\omega F(z)}}\exp\left(\frac{1}{2b\omega F(z)}\right)\left[\operatorname{erf}\left(\frac{1}{\sqrt{2b\omega F(z)}}\right) + \operatorname{erf}\left(\frac{b\omega F(z)t - b - 1}{\sqrt{2b\omega F(z)}}\right)\right]}. \tag{89}$$

The $\mathcal{O}(K)$ equations are solvable but require tedious calculations, especially to determine the required $\frac{\partial^2 T_0^B}{\partial z^2}$, so we do not include the functional form of solutions here, but instead give solutions in integral form in the appendix.

In Figure 11 we compare the leading order asymptotic solutions with the numerical results of the simplified system, at a fixed height in the bottom of the furnace. In Figure 12 we show spatial comparisons for different fixed times. We see that the first order asymptotics capture the main behavior of the numerics at the base but are off by a small error, which we expect would be corrected by finding higher order terms to account for the role of thermal diffusion. The temperature at the top of the furnace is not captured by the leading order asymptotics, since this does not include diffusion and the chosen heat source is close to zero here.

Copyright © by SIAM. Unauthorized reproduction of this article is prohibited.

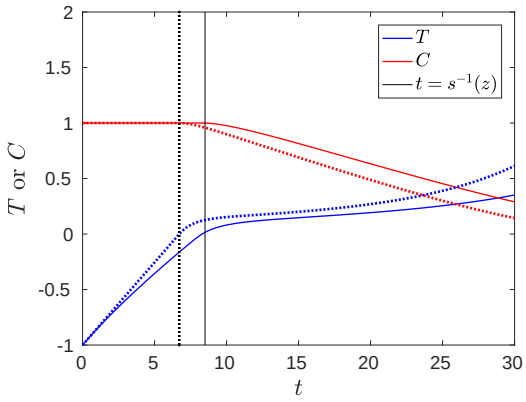

FIG. 11. *Comparison of first order asymptotics, shown in dotted lines, and numerics of the simplified system* (66)–(68)*, shown in solid lines, at height* $z = 0.3$ *for the dimensionless temperature, concentration, and time taken to reach the interface between Regions* A *and* B*. Parameter values used are* $K = 0.01$*,* $\omega = 0.15$*, and* $b = 0.3$*.*

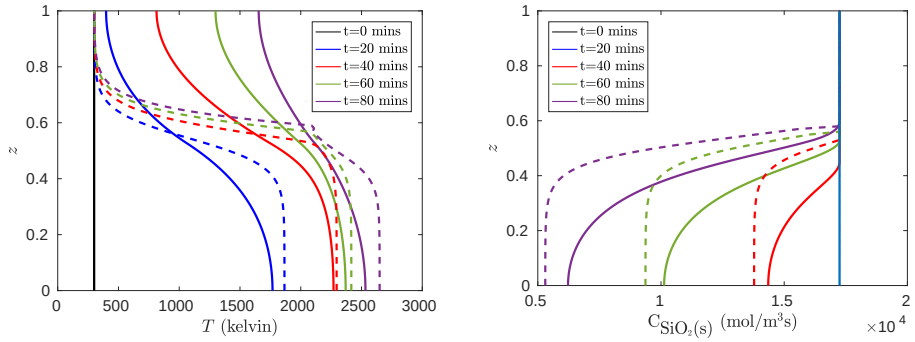

FIG. 12. *Comparison of asymptotics, shown in dotted lines, and numerics of the simplified system* (66)–(68)*, shown in solid lines, for the dimensional temperature (left) and concentration (right). Since the smooth heating source was used the simplified numerics are different from those in Figure* 6*, which use a Heaviside function. Parameter values used are* $K = 0.01$*,* $\omega = 0.15$*, and* $b = 0.3$*.*

4.3. Small heating limit. We can also consider the case where ω is also a small parameter, with $0 < K \ll \omega \ll 1$. Here the heat absorbed by the endothermic reaction between the melted quartz and the carbon is larger than the heat input from the electrode or the induction furnace, but the heat transfer from this source term dominates over diffusion as the main heating mechanism. Asymptotic analysis can be performed with $K = \mathcal{O}(\omega^2)$ and considering the limit $\omega \to 0$. We will not give the details of this analysis here but find behavior in Region A similar to that discussed in the small diffusion limit in section 4.2. The chemical C remains unreacted and the temperature increases due to the heat source $F(z)$, with spatial variation again coming in from derivatives of $F(z)$. The interface $z = s(t)$ can be determined using the same method employed to find (79)–(81), and similar functional forms are found, with the leading order location of the interface being given by the heat source $F(z)$. In Region B the concentration reacts away, with the $\mathcal{O}(1)$ changes found being larger than the $\mathcal{O}(\omega)$ changes in temperature. Since the temperature is small, the dominant

Copyright © by SIAM. Unauthorized reproduction of this article is prohibited.

Downloaded 04/19/18 to 129.67.185.193. Redistribution subject to SIAM license or copyright; see http://www.siam.org/journals/ojsa.php

Downloaded 04/19/18 to 129.67.185.193. Redistribution subject to SIAM license or copyright; see http://www.siam.org/journals/ojsa.php

balance is between the heating and the endothermic reaction. Thus the whole problem is heat controlled and the temperature in the furnace changes to balance the energy input. However, the leading order solution for temperature in Region B blows up in finite time, as temperature changes increase. This issue does not occur in the small diffusion limit in section 4.2, where ω is treated as an $\mathcal{O}(1)$ parameter.

By considering the full model we have reduced the number of equations to a simplified system, which captures the coupled evolution of temperature and concentration of solid quartz in the furnace. This model has two regions of interest: the preheating Region A and the reaction zone Region B. An analytic series solution was found for Region A and the simplified model was considered in the limit of small diffusion, and a small heat source. When diffusion is small, the location of the interface between Regions A and B is determined to leading order by the functional form of the heating source. When the parameter ω is also considered to be small, then the temperature is small in Region B, and the main balance in the problem is between the energy input from the induction furnace and the energy absorbed by the endothermic reaction. Numerical simulations of the simplified model compare well with the full model, so that the simplifications discussed will be useful for future models.

5. Crust formation. We are particularly interested in furnace crust formation, since this slows down the industrials operation and requires "stoking." General insights into this crust can be found from the reaction pathways in (1)–(5), with additional understanding from the analysis of the dimensionless equations with prescribed temperature profile in section 3 and the full model in section 4.

The composition of furnace crust is not well understood [17], and so as a proxy we consider the volume fraction of solid and liquid material, from here on called the solid volume fraction θ_S. This is discussed in more detail in [20]. Note that liquid quartz is highly viscous and can clog up pores in the furnace. Although liquid silicon is less viscous, we include it in the definition for simplicity. We can look at whether the time rate of change of θ_S is positive or negative in the upper part of the furnace, to determine if crust is building up. θ_S is defined as

$$\theta_S = \sum_{\text{solids and liquids i}} \frac{M_{\mathrm{i}}}{\rho_{\mathrm{i}}} \mathrm{C_i} \tag{90}$$

for dimensional $\mathrm{C_i}$, so taking a time derivative we can substitute in the reaction rates from the matrix (6). We can make progress even if we do not define functional forms of the reaction rates or the associated parameter values. This is helpful, since you can still study crust formation regardless of the functional forms chosen. We thus refer to the rates as R_j, as described in (1)–(5). Note that these are dimensional variables. In the upper part of the furnace, where the temperature is too cold for quartz to melt, we impose $R_3 = 0$ to get

$$\begin{aligned} \frac{\partial \theta_S}{\partial t} = {} & \frac{M_{\mathrm{C}}}{\rho_{\mathrm{C}}}(-2R_1 - R_5) + \frac{M_{\mathrm{SiC}}}{\rho_{\mathrm{SiC}}}(R_1 - R_4) + \frac{M_{\mathrm{SiO_2(l)}}}{\rho_{\mathrm{SiO_2(l)}}}(R_2 - R_{-2} - R_5) \\ & + \frac{M_{\mathrm{Si}}}{\rho_{\mathrm{Si}}}(R_2 - R_{-2} - R_4). \end{aligned} \tag{91}$$

In the top of the furnace carbon reacts with the available $\mathrm{SiO_2(l)}$, which is produced from the condensation reaction R_2. Since we expect quantities of Si and $\mathrm{SiO_2(l)}$ to be small compared to the amount of carbon, we can write $R_{-2} \ll R_5$ and $R_5 = R_2$. If we further assume a functional dependence of R_4 on $(P - P_4)^+$, as done in (9), then

Copyright © by SIAM. Unauthorized reproduction of this article is prohibited.

Downloaded 04/19/18 to 129.67.185.193. Redistribution subject to SIAM license or copyright; see http://www.siam.org/journals/ojsa.php

$R_4 = 0$ in the upper part of the furnace, because the partial pressure of SiO is too low. With these assumptions, we can simplify (91) to

$$\frac{\partial \theta_S}{\partial t} = \left(\frac{M_{\mathrm{SiC}}}{\rho_{\mathrm{SiC}}} - 2\frac{M_{\mathrm{C}}}{\rho_{\mathrm{C}}}\right) R_1 + \left(\frac{M_{\mathrm{Si}}}{\rho_{\mathrm{Si}}} - \frac{M_{\mathrm{C}}}{\rho_{\mathrm{C}}}\right) R_2. \tag{92}$$

The molar masses are known constants and can be found with Outokumpu HSC Chemistry for Windows, version 4.0. We take the density of carbon, silicon carbide, and silicon from [10], [14, p. 1086], and [9], respectively. With this data, we have

$$\frac{M_{\mathrm{C}}}{\rho_{\mathrm{C}}} = 5.298 \times 10^{-6}, \quad \frac{M_{\mathrm{SiC}}}{\rho_{\mathrm{SiC}}} = 1.249 \times 10^{-5}, \quad \frac{M_{\mathrm{Si}}}{\rho_{\mathrm{Si}}} = 1.206 \times 10^{-5}. \tag{93}$$

This means that $\frac{\partial \theta_S}{\partial t} > 0$, and as such we will see a buildup of solid in our model. This corresponds in turn to crust formation, regardless of the functional form of reaction rates R_1, R_2, and R_5, and regardless of how large the kinetic parameters are. Notice though that the sign of $\frac{M_{SiC}}{\rho_{SiC}} - 2\frac{M_C}{\rho_C}$ is quite sensitive to the data used in [9] and [10]. A decrease in the value of ρ_C by 15% or an increase in the value of ρ_{SiC} by 18% would change the sign, and it would not then be true that solid always builds up.

We can also incorporate the solutions from section 3, with a prescribed temperature profile $T(z)$. With these we find

$$\begin{aligned} \theta_S &= m_{\mathrm{C}} + \alpha m_{\mathrm{SiO_2(s)}} \\ &+ \epsilon \left[\chi_1 \left(\frac{1}{2} - P_1\right)(m_{\mathrm{SiC}} - 2m_{\mathrm{C}}) + \chi_2 \left(\frac{1}{2} - P_2\right)(m_{\mathrm{Si}} - m_{\mathrm{C}})\right] t + \mathcal{O}(\epsilon^2) \end{aligned} \tag{94}$$

and so can quantify how the crust grows. Taking a spatial partial derivative and using the chain rule, we see

$$\frac{\partial \theta_S}{\partial z} = -\epsilon \left[\chi_1 \frac{dP_1}{dT}(m_{\mathrm{SiC}} - 2m_{\mathrm{C}}) + \chi_2 \frac{dP_2}{dT}(m_{\mathrm{Si}} - m_{\mathrm{C}})\right] \frac{dT}{dz} t + \mathcal{O}(\epsilon^2). \tag{95}$$

Since $\frac{dP_1}{dT}, \frac{dP_2}{dT} > 0$ (see the equilibrium partial pressures figure in [17]) and $\frac{dT}{dz} < 0$ (because of the temperature gradient in the furnace) then

$$\frac{\partial \theta_S}{\partial z} > 0. \tag{96}$$

Hence, the solid volume fraction increases with height in the furnace, according to this model, and the charge is most porous at the lower interface with the gas cavity.

In section 4 the analysis did not consider solid buildup in the upper furnace, since this is an $\mathcal{O}(\epsilon)$ effect when compared to the $\mathcal{O}(1)$ changes taking place in the lower, hotter region. However, we tracked the location of the interface at the base of the charge through the isotherm $T = 0$ (or T=1996 K in dimensional units). This position is largely driven by the external heat source, since diffusion effects are small. Since temperature remains monotone throughout, assuming a monotone heat source F, then to leading order r_1 and r_2 increase with furnace height and thus the rate of crust increase in (92) will increase as well.

6. Discussion. We have investigated asymptotic limits of the silicon furnace model developed in [20], extending the analysis that was undertaken through numerical simulations in that paper. Natural small parameters are the ratio of the timescale for the reaction between carbon and liquid quartz to the timescale for the melting of quartz, and the ratio of timescale of gas advection to the timescale of the melting

Copyright © by SIAM. Unauthorized reproduction of this article is prohibited.

Downloaded 04/19/18 to 129.67.185.193. Redistribution subject to SIAM license or copyright; see http://www.siam.org/journals/ojsa.php

of quartz. With appropriate scalings for the concentrations we have been able to determine the leading order chemical behavior for different spatial regions in the furnace, when a prescribed temperature is imposed in the model. In Region II we find the dominant behavior is solid quartz melting to liquid quartz which then reacts with the available carbon particles to form gaseous CO and SiO. In Region I this SiO gas condenses into silicon and liquid quartz and also reacts with carbon to form silicon carbide and CO. This competition between reactions, determining how much SiC and Si is produced, is represented in the size of the parameter $\lambda = \chi_2/\chi_1$. We have also been able to capture early time behavior in these regions, where the variables move from the initial conditions to typical furnace behavior.

In section 4 we considered asymptotics of the full model with temperature allowed to vary in time. Through systematic reductions we have derived a simplified system of two coupled equations for temperature and the concentration of solid quartz, which depends on three parameters, 10 times fewer than the number used in the full model. These three parameters represent the heating from the external source, the thermal diffusion, and the rate of melting of solid quartz. Numerical simulations of the simplified system compare well the full model, showing the same qualitative behavior. We find asymptotic solutions to the reduced system, treating the diffusivity, K, as a small parameter. The leading order solutions, where no diffusion occurs, are representative of the behavior in the reaction zone. This suggests that the dominant heat transfer mechanisms are the energy input from the induction furnace into the pilot furnace, and the heat absorption of the endothermic reaction between carbon and quartz. The pilot furnace is most thermally conductive along the graphite walls, since conduction between solid particles is relatively small. In an industrial furnace the subdominance of diffusion is likely to be even more pronounced, since energy is input directly from the electrodes.

By examining crust formation in section 5, we found crust builds up in this model regardless of the functional forms or kinetic parameters of reaction rates R_1 and R_2. However, the model assumes that there is no solid or liquid motion and that everywhere in the furnace there is a mixture of solid, liquid, and gas. In practice liquid silicon is inviscid and so will drip to the crater when produced. This would have an impact on crust formation, as silicon would not contribute to the solid fraction in the upper furnace, as it does in (92). In addition, the porosity will become so low at the bottom of the charge that solid and liquid material will fall to the furnace base. Clearly there needs to be a failure criterion for this falling material. One possibility is to use the melting isotherm, so that all material hotter than this will have fallen to the base. The reduced system in section 4 will be useful when further physical effects are incorporated in future models, such as the dripping of inviscid silicon, the falling of material from the charge to the crater, and the two-dimensional mechanical bridging of the crust.

Appendix: Asymptotic expansions. Here we list asymptotic solutions to leading and first order for each subproblem considered. For simplicity in the prescribed temperature asymptotics we expand the gas flux as one variable, so that $U_g \mathrm{C}_g = U_g^0 \mathrm{C}_g^0 + \epsilon U_g^1 \mathrm{C}_g^1 + \mathcal{O}(\epsilon^2)$. If instead we used individual expansions $U_g = U_g^0 + \epsilon U_g^1 + \mathcal{O}(\epsilon^2)$, $\mathrm{C}_g = \mathrm{C}_g^0 + \epsilon \mathrm{C}_g^1 + \mathcal{O}(\epsilon^2)$, then the leading order asymptotics remain the same, but there will be more complex relationships for the first order terms, which include the algebraic no voids condition. For brevity we suppress the notation $T(z)$ and $P_i(T(z))$ to T and P_i, respectively, unless we are integrating over a dummy variable.

Copyright © by SIAM. Unauthorized reproduction of this article is prohibited.

Downloaded 04/19/18 to 129.67.185.193. Redistribution subject to SIAM license or copyright; see http://www.siam.org/journals/ojsa.php

Prescribed temperature—Region IIa. On the early timescale $\hat{t} = t/\epsilon$ the solid and liquid concentrations are given by

$$\mathrm{C_C} = 1 + \epsilon\alpha\,(T - T_m)\left(\hat{t} + e^{-\hat{t}} - 1\right) + \mathcal{O}(\epsilon^2), \tag{97}$$

$$\mathrm{C_{SiC}} = \epsilon\chi_1\left(\frac{1}{2} - P_1\right)\hat{t} + \mathcal{O}(\epsilon^2), \tag{98}$$

$$\mathrm{C_{SiO_2(s)}} = \alpha - \epsilon\alpha\,(T - T_m)\,\hat{t} + \mathcal{O}(\epsilon^2), \tag{99}$$

$$\begin{aligned}\mathrm{C_{SiO_2(l)}} = {}& \alpha\,(T - T_m)\left(1 - e^{-\hat{t}}\right) + \epsilon\Bigg(\chi_2\left(\frac{1}{2} - P_2\right)^{+}\left(1 - e^{-\hat{t}}\right) - \alpha\,(T - T_m)^2 \\ & \times\left(\hat{t} - 1 + e^{-\hat{t}}\right) - \alpha^2\,(T - T_m)^2\left(\hat{t} - 2 + e^{-\hat{t}}\left(-\frac{\hat{t}^2}{2} + 2\hat{t} + 1\right) + e^{-2\hat{t}}\right)\Bigg) + \mathcal{O}(\epsilon^2),\end{aligned} \tag{100}$$

$$\mathrm{C_{Si}} = \epsilon\chi_2\left(\frac{1}{2} - P_2\right)^{+}\hat{t} + \mathcal{O}(\epsilon^2). \tag{101}$$

The gas flux and partial pressure are found to be

$$U_g\mathrm{C}_g = 2\alpha\left(1 - e^{-\hat{t}}\right)\int_{y=0}^{y=z}(T(y) - T_m)dy + 2\epsilon\int_{y=0}^{y=z} r^1_{5,IIa}(\hat{t}, y) - r^0_{2,IIa}(\hat{t}, y)dy + \mathcal{O}(\epsilon^2), \tag{102}$$

$$P = \frac{1}{2} - \epsilon\frac{\int_{y=0}^{y=z} r^0_{1,IIa}(\hat{t}, y) + r^0_{2,IIa}(\hat{t}, y)dy}{U^0_g\mathrm{C}^0_g} + \mathcal{O}(\epsilon^2) \quad \text{for } U^0_g\mathrm{C}^0_g \neq 0, \text{ i.e., } \hat{t}, z > 0, \tag{103}$$

where $U^0_g\mathrm{C}^0_g$ is the leading term in (102), and

$$r^0_{1,IIa}(\hat{t}, z) = \chi_1\left(\frac{1}{2} - P_1\right), \quad r^0_{2,IIa} = \chi_2\left(\frac{1}{2} - P_2\right)^{+}, \tag{104}$$

$$\begin{aligned} r^1_{5,IIa} = {}& \alpha^2\,(T - T_m)^2\left(\hat{t} + e^{-\hat{t}} - 1\right)\left(1 - e^{-\hat{t}}\right) + \Bigg(\chi_2\left(\frac{1}{2} - P_2\right)^{+}\left(1 - e^{-\hat{t}}\right) \\ & - \alpha\,(T - T_m)^2\left(\hat{t} - 1 + e^{-\hat{t}}\right) - \alpha^2\,(T - T_m)^2 \\ & \left(\hat{t} - 2 + e^{-\hat{t}}\left(-\frac{\hat{t}^2}{2} + 2\hat{t} + 1\right) + e^{-2\hat{t}}\right)\Bigg).\end{aligned} \tag{105}$$

Prescribed temperature—Region IIb. Since several of the higher order terms in this region can only be written in terms of integrals, we give the $\mathcal{O}(1)$ terms and then the $\mathcal{O}(\epsilon)$ terms. Note that

$$\mathrm{C_{SiO_2(s)}} = \alpha e^{-(T - T_m)t}, \tag{106}$$

and so there in no correction term needed for the concentration of solid quartz. Five of the leading order variables are easily found as

$$\mathrm{C}^0_{\mathrm{C}} = \alpha e^{-(T - T_m)t} + (1 - \alpha), \tag{107}$$

Copyright © by SIAM. Unauthorized reproduction of this article is prohibited.

$$\mathrm{C}^0_{\mathrm{SiO_2(l)}} = \frac{(T-T_m)\alpha e^{-(T-T_m)t}}{\alpha e^{-(T-T_m)t} + (1-\alpha)}, \tag{108}$$

$$\mathrm{C}^0_{\mathrm{SiO_2(s)}} = \alpha e^{-(T-T_m)t}, \tag{109}$$

$$U^0_g \mathrm{C}^0_g = 2\alpha \int_{y=0}^{y=z} e^{-(T(y)-T_m)t}\,(T(y)-T_m)\,dy, \tag{110}$$

$$P^0 = \frac{1}{2}. \tag{111}$$

The solutions for $\mathrm{C}^0_{\mathrm{SiC}}$ and $\mathrm{C}^0_{\mathrm{Si}}$ are different in the temperature regions $P_2, P_4 \geq \frac{1}{2}$, $P_2 < \frac{1}{2} \leq P_4$, and $P_4 < \frac{1}{2} \leq P_2$. Note that there is no region in $T > T_m$ where P_2 and P_4 are both less than $\frac{1}{2}$

In $P_2 < \frac{1}{2} \leq P_4$ we have

$$\mathrm{C}^0_{\mathrm{SiC}} = \chi_1 \left(\frac{1}{2} - P_1\right) \left(\frac{\alpha}{T-T_m}\left(1 - e^{-(T-T_m)t}\right) + (1-\alpha)t\right), \tag{112}$$

$$\mathrm{C}^0_{\mathrm{Si}} = \chi_2 \left(\frac{1}{2} - P_2\right) \left(\alpha e^{-(T-T_m)t} + (1-\alpha)\right)^{\chi_{-2}} \int_{\tilde{t}=0}^{t=\tilde{t}} \left(\alpha e^{-(T-T_m)\tilde{t}} + (1-\alpha)\right)^{-\chi_{-2}} d\tilde{t}. \tag{113}$$

In $P_2, P_4 \geq \frac{1}{2} =$ we have that $\mathrm{C}^0_{\mathrm{SiC}}$ is given by (112) and that $\mathrm{C}^0_{\mathrm{Si}} = 0$. In $P_4 < \frac{1}{2} \leq P_2$

$$\mathrm{C}^0_{\mathrm{SiC}} = \begin{cases} \chi_1\left(\frac{1}{2}-P_1\right)\left[\frac{\alpha(e^{-(T-T_m)t} - e^{-\chi_4(\frac{1}{2}-P_4)t})}{\chi_4(\frac{1}{2}-P_4)-(T-T_m)} + \frac{1-\alpha}{\chi_4(\frac{1}{2}-P_4)}\left(1 - e^{-\chi_4(\frac{1}{2}-P_4)t}\right)\right], \\ \qquad\qquad \chi_4(\frac{1}{2}-P_4) \neq (T-T_m), \\ \chi_1\left(\frac{1}{2}-P_1\right)\left[\alpha t + \frac{1-\alpha}{\chi_4(\frac{1}{2}-P_4)}\left(1 - e^{-\chi_4(\frac{1}{2}-P_4)t}\right)\right], \\ \qquad\qquad \chi_4(\frac{1}{2}-P_4) = (T-T_m), \end{cases} \tag{114}$$

$$\mathrm{C}^0_{\mathrm{Si}} = 2\chi_4 \left(\frac{1}{2} - P_4\right) \left(\alpha e^{-(T-T_m)t} + (1-\alpha)\right)^{\chi_{-2}} \int_{\tilde{t}=0}^{t=\tilde{t}} \frac{\mathrm{C}^0_{\mathrm{SiC}}(\tilde{t}, z)}{\left(\alpha e^{-(T-T_m)\tilde{t}} + (1-\alpha)\right)^{\chi_{-2}}} d\tilde{t}. \tag{115}$$

To find $\mathrm{C}^1_{\mathrm{C}}$ we note that

$$\frac{\partial \mathrm{C}^1_{\mathrm{C}}}{\partial t} = \frac{\partial \mathrm{C}^0_{\mathrm{SiO_2(l)}}}{\partial t} - 2r^0_1 - r^0_2 - r^0_{-2}, \tag{116}$$

which we can integrate to give

$$\begin{aligned} \mathrm{C}^1_{\mathrm{C}} = {} & \mathrm{C}^0_{\mathrm{SiO_2(l)}} - (T-T_m)\alpha - \chi_2\left(\frac{1}{2} - P_2\right)t \\ & + \int_{\tilde{t}=0}^{\tilde{t}=t} -2\mathrm{C}^0_{\mathrm{C}}(\tilde{t}, z)\left(\frac{1}{2} - P_1\right) + \chi_{-2}\mathrm{C}^0_{\mathrm{SiO_2(l)}}(\tilde{t}, z)\mathrm{C}^0_{\mathrm{Si}}(\tilde{t}, z)d\tilde{t}. \end{aligned} \tag{117}$$

The other $\mathcal{O}(\epsilon)$ terms are found to be

$$\begin{aligned} \mathrm{C}^1_{\mathrm{SiO_2(l)}} = \frac{1}{\mathrm{C}^0_{\mathrm{C}}} \Bigg(& \frac{\alpha(1-\alpha)(T-T_m)^2 e^{(T-T_m)t}}{\left(\alpha + (1-\alpha)e^{(T-T_m)t}\right)^2} \\ & + \chi_2\left(\frac{1}{2} - P_2\right)^+ - \chi_{-2}\mathrm{C}^0_{\mathrm{SiO_2(l)}}\mathrm{C}^0_{\mathrm{Si}} - \mathrm{C}^0_{\mathrm{SiO_2(l)}}\mathrm{C}^1_{\mathrm{C}}\Bigg), \end{aligned} \tag{118}$$

Copyright © by SIAM. Unauthorized reproduction of this article is prohibited.

Downloaded 04/19/18 to 129.67.185.193. Redistribution subject to SIAM license or copyright; see http://www.siam.org/journals/ojsa.php

Downloaded 04/19/18 to 129.67.185.193. Redistribution subject to SIAM license or copyright; see http://www.siam.org/journals/ojsa.php

(119)
$$U_g^1 \mathrm{C}_g^1 = 2\int_{y=0}^{y=z} \Big[\mathrm{C}^1_{\mathrm{SiO_2(l)}}(t,y)\mathrm{C}^0_{\mathrm{C}}(t,y) + \mathrm{C}^0_{\mathrm{SiO_2(l)}}(t,y)\mathrm{C}^1_{\mathrm{C}}(t,y) - \chi_2 \left(\frac{1}{2} - P_2\right)^+ + \chi_{-2}\mathrm{C}^0_{\mathrm{SiO_2(l)}}(t,y)\mathrm{C}^0_{\mathrm{Si}}(t,y)\Big] dy,$$

(120)
$$P^1 = \frac{1}{U_g^0 \mathrm{C}_g^0}\int_{y=0}^{y=z} \Big[-\chi_1 \mathrm{C}^0_{\mathrm{C}}(t,y)\left(\frac{1}{2} - P_1(T(y))\right) - \chi_2 \left(\frac{1}{2} - P_2(T(y))\right)^+ + \chi_{-2}\mathrm{C}^0_{\mathrm{SiO_2(l)}}(t,y)\mathrm{C}^0_{\mathrm{Si}}(t,y) - \chi_4 \mathrm{C}^0_{\mathrm{SiC}}(t,y)\left(\frac{1}{2} - P_4(T(y))\right)^+ \Big] dy,$$

(121)
$$\mathrm{C}^1_{\mathrm{SiC}} = \begin{cases} \chi_1 \int_{\tilde{t}=0}^{\tilde{t}=t} \mathrm{C}^0_{\mathrm{C}}(\tilde{t},z)P^1(\tilde{t},y) + \mathrm{C}^1_{\mathrm{C}}(\tilde{t},z)\left(\frac{1}{2} - P_1\right) d\tilde{t}, & P_4 \geq \frac{1}{2}, \\ e^{-\chi_4(\frac{1}{2}-P_4)t}\int_{\tilde{t}=0}^{\tilde{t}=t} e^{\chi_4(\frac{1}{2}-P_4)\tilde{t}}\left(\chi_1 \mathrm{C}^0_{\mathrm{C}}(\tilde{t},z)P^1(\tilde{t},y) + \chi_1 \mathrm{C}^1_{\mathrm{C}}(\tilde{t},z)\left(\frac{1}{2} - P_1\right) - \chi_4 \mathrm{C}^0_{\mathrm{SiC}}P^1\right) d\tilde{t}, & P_4 < \frac{1}{2}, \end{cases}$$

(122)
$$\mathrm{C}^1_{\mathrm{Si}} = \left(\alpha e^{-(T-T_m)t} + 1 - \alpha\right)^{\chi_{-2}} \int_{\tilde{t}=0}^{\tilde{t}=t} \Big[\left(\alpha e^{-(T-T_m)\tilde{t}} + 1 - \alpha\right)^{-\chi_{-2}} \Big(\chi_2 P^1(\tilde{t},z)\mathbf{1}_{\{P_2 \leq \frac{1}{2}\}} - \chi_{-2}\mathrm{C}^1_{\mathrm{SiO_2(l)}}(\tilde{t},z)\mathrm{C}^0_{\mathrm{Si}}(\tilde{t},z) + \chi_4 \mathrm{C}^1_{\mathrm{SiC}}(\tilde{t},z)\left(\frac{1}{2} - P_4\right)^+ + \chi_4 \mathrm{C}^0_{\mathrm{SiC}}(\tilde{t},z)P^1(\tilde{t},z)\mathbf{1}_{\{P_4 \leq \frac{1}{2}\}} \Big) \Big] d\tilde{t}.$$

Prescribed temperature—Region Ia.

(123)
$$\mathrm{C_C} = 1 + \mathcal{O}(\epsilon^2),$$

(124)
$$\mathrm{C_{SiC}} = \epsilon\chi_1\left(\frac{1}{2} - P_1\right)\hat{t} + \mathcal{O}(\epsilon^2),$$

(125)
$$\mathrm{C_{SiO_2(s)}} = \alpha,$$

(126)
$$\mathrm{C_{SiO_2(l)}} = \epsilon\chi_2\left(\frac{1}{2} - P_2\right)\left(1 - e^{-\hat{t}}\right) + \mathcal{O}(\epsilon^2),$$

(127)
$$\mathrm{C_{Si}} = \epsilon\chi_2\left(\frac{1}{2} - P_2\right)\hat{t} + \mathcal{O}(\epsilon^2),$$

(128)
$$U_g \mathrm{C}_g = U^0_{g,IIa}\mathrm{C}^0_{g,IIa}(\hat{t},z_m) + \epsilon\left(2\int_{y=z_m}^{y=z} r^1_{5,Ia}(\hat{t},y) - r^0_{2,Ia}(\hat{t},y)dy + U^1_{g,IIa}\mathrm{C}^1_{g,IIa}(\hat{t},z_m)\right) + \mathcal{O}(\epsilon^2),$$

(129)
$$P = \frac{1}{2} - \epsilon\left(\frac{\int_{y=z_m}^{y=z} r^0_{1,Ia}(\hat{t},y) + r^0_{2,Ia}(\hat{t},y)dy}{U^1_{g,IIa}\mathrm{C}^1_{g,IIa}(t,z_m)} - P^1_{IIa}(\hat{t},z_m)\right) + \mathcal{O}(\epsilon^2),$$

Copyright © by SIAM. Unauthorized reproduction of this article is prohibited.

Downloaded 04/19/18 to 129.67.185.193. Redistribution subject to SIAM license or copyright; see http://www.siam.org/journals/ojsa.php

where the functions $U^0_{g,IIa}\mathrm{C}^0_{g,IIa}$ and $U^1_{g,IIa}\mathrm{C}^1_{g,IIa}$ are the $\mathcal{O}(1)$ and $\mathcal{O}(\epsilon)$ terms in (102), P^1_{IIa} is the $\mathcal{O}(\epsilon)$ term in (103), and the reaction rates are given by

(130)
$$r^0_{1,Ia}(\hat{t},z)=\chi_1\left(\frac{1}{2}-P_1\right),\ \ r^0_{2,Ia}=\chi_2\left(\frac{1}{2}-P_2\right),\ \ r^1_{5,Ia}=\chi_2\left(\frac{1}{2}-P_2\right)\left(1-e^{-\hat{t}}\right).$$

Prescribed temperature—Region Ib. In this region we have solutions

$$\mathrm{C_C}=1-\epsilon\left(2\chi_1\left(\frac{1}{2}-P_1\right)+\chi_2\left(\frac{1}{2}-P_2\right)\right)t+\mathcal{O}(\epsilon^2), \tag{131}$$

$$\mathrm{C_{SiO_2(s)}}=\alpha, \tag{132}$$

$$\mathrm{C_{SiO_2(l)}}=\epsilon\chi_2\left(\frac{1}{2}-P_2\right)+\mathcal{O}(\epsilon^2), \tag{133}$$

$$U_g\mathrm{C}_g=U^0_{g,IIb}\mathrm{C}^0_{g,IIb}(t,z_m)+\epsilon U^1_{g,IIb}\mathrm{C}^1_{g,IIb}(t,z_m)+\mathcal{O}(\epsilon^2), \tag{134}$$

where $U^0_{g,IIb}\mathrm{C}^0_{g,IIb}$ and $U^1_{g,IIb}\mathrm{C}^1_{g,IIb}$ are the functions in Region IIb, given in (110) and (119), respectively. We also have

(135)
$$P=\frac{1}{2}+\epsilon\left(P^1_{IIa}(t,z_m)-\frac{\int_{y=z_m}^{y=z}\chi_1\left(\frac{1}{2}-P_1(T(y))\right)+\chi_2\left(\frac{1}{2}-P_2(T(y))\right)dy}{U^0_{g,IIb}\mathrm{C}^0_{g,IIb}(t,z_m)}\right)+\mathcal{O}(\epsilon^2),$$

$$\begin{aligned}\mathrm{C_{SiC}}=\chi_1\left(\frac{1}{2}-P_1\right)t+\epsilon\Bigg(&\chi_1\int_{\tilde{t}=0}^{\tilde{t}=t}P^1(\tilde{t},z)d\tilde{t}-\Bigg(\chi_1^2\left(\frac{1}{2}-P_1\right)^2\\&+\frac{\chi_1\chi_2}{2}\left(\frac{1}{2}-P_1\right)\left(\frac{1}{2}-P_2\right)\Bigg)t^2\Bigg)+\mathcal{O}(\epsilon^2),\end{aligned} \tag{136}$$

where P^1 is the $\mathcal{O}(\epsilon)$ term in (135). We also have

(137)
$$\mathrm{C_{Si}}=\chi_2\left(\frac{1}{2}-P_2\right)t+\epsilon\left(\int_{\tilde{t}=0}^{\tilde{t}=t}\chi_2P^1(\tilde{t},z)d\tilde{t}-\frac{\chi_{-2}\chi_2^2}{2}\left(\frac{1}{2}-P_2\right)^2t^2\right)+\mathcal{O}(\epsilon^2).$$

Full model asymptotics—small diffusion limit. Expanding variables in terms of K we have in Region A

$$T^A(z,t)=-1+\omega F(z)t+\omega\sum_{n=1}^{\infty}K^nF^{(2n)}(z)\frac{t^{n+1}}{(n+1)!},\ \ C^A(z,t)=0, \tag{138}$$

and that the position of the interface is given by

(139)
$$\begin{aligned}s(t)=F^{-1}\left(\frac{1}{\omega t}\right)&-\frac{K}{2}\frac{F''(s_0(t))}{F'(s_0(t))}t\\&+K^2\left(\frac{F''(s_0(t))F'''(s_0(t))}{4(F'(s_0(t)))^2}-\frac{F^{IV}(s_0(t))}{6F'(s_0(t))}-\frac{(F''(s_0(t)))^3}{8(F'(s_0(t)))^3}\right)t^2+\mathcal{O}(K^3).\end{aligned}$$

Copyright © by SIAM. Unauthorized reproduction of this article is prohibited.

Downloaded 04/19/18 to 129.67.185.193. Redistribution subject to SIAM license or copyright; see http://www.siam.org/journals/ojsa.php

In Region B we have the leading order terms

(140)
$$C_0^B(z,t) = \frac{\exp\left(-\frac{2+b}{2\omega F(z)} + (b+1)\,t - \frac{b\omega F(z)}{2}t^2\right)}{1 + \sqrt{\frac{\pi}{2b\omega F(z)}}\exp\left(\frac{1}{2b\omega F(z)}\right)\left[\operatorname{erf}\left(\frac{1}{\sqrt{2b\omega F(z)}}\right) + \operatorname{erf}\left(\frac{b\omega F(z)t-b-1}{\sqrt{2b\omega F(z)}}\right)\right]},$$

(141)
$$T_0^B = \frac{1}{b}(C_0^B - 1) - 1 + \omega F(z)t.$$

The first order terms satisfy equations

(142)
$$b\frac{\partial T_1^B}{\partial t} - \frac{\partial C_1^B}{\partial t} = b\frac{\partial^2 T_0^B}{\partial z^2}, \quad \frac{\partial C_1}{\partial t} = -b(C_0^B T_1^B + C_1^B T_0^B)$$

with initial conditions

(143)
$$T_1^B + s_1(t)\frac{\partial T_0^B}{\partial z} = 0, \quad C_1^B + s_1(t)\frac{\partial C_0^B}{\partial z} = 0 \quad \text{on } t = \frac{1}{\omega F(z)}.$$

We can integrate the first equation in (142) to obtain

(144)
$$T_1^B = \frac{1}{b}C_1^B + \frac{F''(z)}{2\omega F(z)^2} + \int_{\tilde{t}=1/\omega F(z)}^{\tilde{t}=t} \frac{\partial^2 T_0^B}{\partial z^2}(z,\tilde{t})d\tilde{t},$$

where the spatial function $F''(z)/2\omega F(z)^2$ has been determined using (143), (86), and (80), with $s_0(t) = z$ and $t = 1/\omega F(z)$. Equation (144) can be substituted into the second equation in (142) to find

$$C_1^B(z,t) = \frac{1}{I(z,t)}\int_{\tilde{t}=1/\omega F(z)}^{\tilde{t}=t} I(z,\tilde{t})\left[-\frac{bC_0^B(z,\tilde{t})F''(z)}{2\omega F(z)^2} - bC_0^B(z,\tilde{t})\int_{u=1/\omega F(z)}^{u=\tilde{t}} \frac{\partial^2 T_0^B}{\partial z^2}(z,u)du\right]d\tilde{t} + \frac{I(z,(\omega F(z))^{-1})}{I(z,t)}\frac{F''(z)}{2\omega F'(z)F(z)}\left.\frac{\partial C_0^B}{\partial z}\right|_{t=(\omega F(z))^{-1}},$$

where the integrating factor I is given by

(145)
$$I(z,t) = \exp\left(\int^{\tilde{t}=t} bT_0^B(z,\tilde{t}) + C_0^B(z,\tilde{t})d\tilde{t}\right).$$

The solution in (145) can then be substituted into (144) to determine T_1^B.

Acknowledgments. The authors thank Aasgeir Valderhaug, Rolf Birkeland, and Harald Wegge (all at Elkem) for helpful discussions regarding this work. The first author thanks Elkem for the opportunity for on-site work during parts of this research.

REFERENCES

[1] J. T. Abrahamson and M. S. Strano, *Analytical solution to coupled chemical reaction and thermally diffusing systems: Applicability to self-propagating thermopower waves*, J. Phys. Chem. Lett., 1 (2010), pp. 3514–3519.

[2] B. Andresen, *Process Model for Carbothermic Production of Silicon Metal*, Ph.D. thesis, Norwegian Institute of Technology, Trondheim, 1995.

Copyright © by SIAM. Unauthorized reproduction of this article is prohibited.

[3] E. S. Antoniou, J. K. Bechtold, and M. Matalon, *A diffusional-thermal theory of near-stoichiometric premixed flames*, SIAM J. Appl. Math., 64 (2004), pp. 1434–1456.
[4] H. M. Byrne and J. Norbury, *Stable solutions for a catalytic converter*, SIAM J. Appl. Math., 54 (1994), pp. 789–813.
[5] N. T. Fadai, C. P. Please, and R. A. Van Gorder, *Asymptotic analysis of a multi-phase drying model motivated by coffee bean roasting*, SIAM J. Appl. Math., 78 (2018), pp. 418–436.
[6] N. D. Fowkes and A. P. Bassom, *Batch processing in a glass furnace*, ANZIAM J., 57 (2015), pp. 175–188.
[7] V. V. Gubernov, J. J. Sharples, H. S. Sidhu, A. C. McIntosh, and J. Brindley, *Properties of combustion waves in the model with competitive exo-and endothermic reactions*, J. Math. Chem., 50 (2012), pp. 2130–2140.
[8] S. A. Halvorsen, A. Schei, and J. H. Downing, *A unidimensional dynamic model for the (ferro)silicon process*, in Electric Furnace Conference Proceedings, Vol. 50, ISS/AIME, 1992, pp. 45–59.
[9] D. R. Lide, ed., *CRC Handbook of Chemistry and Physics*, 84th ed., CRC Press, Boca Raton, FL, 2003.
[10] D. R. Lide, ed., *CRC Handbook of Chemistry and Physics*, 86th ed., CRC Press, Boca Raton, FL, 2005.
[11] B. F. Lund, *Rigorous Simulation Models for Improved process operation*, Ph.D. thesis, Norwegian University of Science and Technology, Trondheim, 2005.
[12] B. P. Marchant and J. Norbury, *Discontinuous travelling wave solutions for certain hyperbolic systems*, IMA J. Appl. Math., 67 (2002), pp. 201–224.
[13] J. Norbury and A. M. Stuart, *A model for porous-medium combustion*, Quart. J. Mech. Appl. Math., 42 (1989), pp. 159–178.
[14] P. Patnaik, *Handbook of Inorganic Chemical Compounds*, McGraw-Hill, New York, 2002.
[15] C. P. Please, P. S. Hagan, and D. W. Schwendeman, *Light-off behavior of catalytic converters*, SIAM J. Appl. Math., 54 (1994), pp. 72–92.
[16] C. P. Please, F. Liu, and D. L. S. McElwain, *Condensed phase combustion travelling waves with sequential exothermic or endothermic reactions*, Combust. Theory Model., 7 (2003), pp. 129–143.
[17] A. Schei, J. K. Tuset, and H. Tveit, *Production of High Silicon Alloys*, Tapir, Trondheim, Norway, 1998.
[18] L. A. Segel and M. Slemrod, *The quasi-steady-state assumption: A case study in perturbation*, SIAM Rev., 31 (1989), pp. 446–477.
[19] J. J. Sharples, H. S. Sidhu, A. C. McIntosh, J. Brindley, and V. Gubernov, *Analysis of combustion waves arising in the presence of a competitive endothermic reaction*, IMA J. Appl. Math., 77 (2012), pp. 18–31.
[20] B. M. Sloman, C. P. Please, R. A. Van Gorder, A. M. Valderhaug, R. G. Birkeland, and H. Wegge, *A heat and mass transfer model of a silicon pilot furnace*, Metallurgical Materials Trans. B, 48 (2017), pp. 2664–2676.
[21] A. M. Valderhaug, *Modelling and Control of Submerged-Arc Ferrosilicon Furnaces*, Ph.D. thesis, Norwegian Institute of Technology, Trondheim, 1992.
[22] S. O. Wasbø and A. Hammervold, SiMod–A Silicon Furnace Process Model, *Private communication*, 2014.
[23] W. Wee, H. Sidhu, J. Sharples, I. Towers, and V. Gubernov, *Properties of reaction fronts in a non-adiabatic two stage exothermic-endothermic competitive reaction scheme*, ANZIAM J., 54 (2013), pp. 646–663.

Downloaded 04/19/18 to 129.67.185.193. Redistribution subject to SIAM license or copyright; see http://www.siam.org/journals/ojsa.php

Copyright © by SIAM. Unauthorized reproduction of this article is prohibited.